Available online at www.sciencedirect.com

ScienceDirect

Geochimica et Cosmochimica Acta 271 (2020) 194–211

Geochimica et Cosmochimica Acta

www.elsevier.com/locate/gca

Anomalous ^{182}W in high $^{3}He/^{4}He$ ocean island basalts: Fingerprints of Earth's core?

A. Mundl-Petermeier [a,b,*], R.J. Walker [a], R.A. Fischer [c], V. Lekic [a], M.G. Jackson [d], M.D. Kurz [e]

[a] Department of Geology, University of Maryland, College Park, USA
[b] Department of Lithospheric Research, University of Vienna, Vienna, Austria
[c] Department of Earth & Planetary Sciences, Harvard University, Cambridge, MA, USA
[d] Department of Earth Science, University of California Santa Barbara, USA
[e] Woods Hole Oceanographic Institution, Woods Hole, USA

Received 5 August 2019; accepted in revised form 16 December 2019; Available online 24 December 2019

Abstract

The short-lived ^{182}Hf-^{182}W isotope system ($t_{1/2} = 9$ Ma) left evidence in both ancient and modern terrestrial rock record of processes that took place during the earliest stages of Earth's accretionary and differentiation history. We report $\mu^{182}W$ values (the deviation of $^{182}W/^{184}W$ of a sample from that of laboratory standards, in parts per million) and corresponding $^{3}He/^{4}He$ ratios for rocks from 15 different hotspots. These rocks are characterized by $\mu^{182}W$ values that range from ~0 to as low as -23 ± 4.5. For each volcanic system that includes rocks with negative $\mu^{182}W$ values, the values tend to be negatively correlated with $^{3}He/^{4}He$. The W-He isotopic characteristics of all samples can be successfully modeled via mixing involving at least three mantle source reservoirs with distinct $\mu^{182}W$-$^{3}He/^{4}He$ characteristics. One reservoir has $^{3}He/^{4}He \approx 8$ R/R_A and $\mu^{182}W \approx 0$, which is indistinguishable from the convecting upper mantle. Based on high $^{3}He/^{4}He$, the other two reservoirs are presumed to be relatively un-degassed and likely primordial. One reservoir is characterized by $\mu^{182}W \approx 0$, while the other is characterized by $\mu^{182}W \leq -23$. The former reservoir likely formed from a silicate differentiation process more than 60 Myr after the origin of the solar system, but has remained partially or wholly isolated from the rest of the mantle for most of Earth history. The latter reservoir most likely includes a component that formed while ^{182}Hf was extant. Mass balance constraints on the isotopic composition of the core suggest it has a strongly negative $\mu^{182}W$ value of ~−220. Thus, it is a candidate for the origin of the negative $\mu^{182}W$ in the plume sources. Mixing models show that the direct addition of outer core metal into a plume rising from the core-mantle boundary would result in collateral geochemical effects, particularly in the abundances of highly siderophile elements, which are not observed in OIB. Instead, the reservoir characterized by negative $\mu^{182}W$ most likely formed in the lowermost mantle as a result of core-mantle isotopic equilibration. The envisioned equilibration process would raise the W concentration and lower the $\mu^{182}W$ of the resulting silicate reservoir, relative to the rest of the mantle. The small proportion (<0.3 %) of this putative core-mantle equilibrated reservoir required to account for the $\mu^{182}W$ signatures observed in OIB is insufficient to result in observable effects on most other elemental and/or isotopic compositions. The presumed primordial reservoirs may be linked to seismically distinct regions in the lower mantle. Seismically imaged mantle plumes appear to preferentially ascend from the vicinity of large low-shear velocity provinces (LLSVPs), which have been interpreted as thermochemical piles. We associate the LLSVPs with the primordial reservoir characterized by high $^{3}He/^{4}He$ and $\mu^{182}W = 0$. Smaller, ultra-low velocity zones (ULVZs) present at the core-mantle boundary have been interpreted to

* Corresponding author at: Department of Lithospheric Research, University of Vienna, Vienna, Austria.
E-mail address: andrea.mundl@univie.ac.at (A. Mundl-Petermeier).

https://doi.org/10.1016/j.gca.2019.12.020

consist of (partially) molten lower mantle material. The negative $\mu^{182}W$ signatures observed in some plume-derived lavas may result from small contributions of ULVZ material that has inherited its negative $\mu^{182}W$ signature through core-mantle equilibration.

Keywords: OIB; $\mu^{182}W$; $^{3}He/^{4}He$; Core-mantle interaction; Mantle plumes; ULVZ; LLSVP

1. INTRODUCTION

Ocean island basalts (OIB) are a global volcanic feature of the modern Earth. Most OIB result from intraplate volcanism transiting oceanic lithosphere. Based on estimated potential temperatures of their mantle sources, OIB have also been associated with so-called mantle hotspots. Consequently, OIB are commonly presumed to form as a result of decompression melting of rising mantle plumes that most likely originated at major thermal boundary layers in the mantle. The inferred thermal and chemical structures of mantle plumes suggest they may entrain material from various depths in the mantle, including diverse materials potentially from near or at the core-mantle boundary (CMB) (e.g., Weis et al., 2011; Farnetani et al., 2012). Numerous studies of long-lived radiogenic isotope systems and noble gases in OIB have concluded that OIB sources contain a variety of materials that have been recycled back into the mantle from the Earth's surface throughout most of Earth history, as well as primitive, less-degassed mantle (e.g., Hofmann and White, 1982; Kurz et al., 1982; Zindler and Hart, 1986; Hauri and Hart, 1993; Hofmann, 1997, Graham, 2002). Consistent with these concepts, seismic tomography studies have imaged structures in both the upper and lower mantle interpreted to be mantle plumes, characterized by contrasting temperatures, compositions, or a combination of both, relative to the ambient mantle (e.g., Montelli et al., 2004; French and Romanowicz, 2015).

Since the 1960s, much effort has been directed at deciphering the processes at work over Earth history that have led to the chemical, and particularly the long-lived radiogenic isotopic, characteristics of OIB (e.g., Gast et al., 1964; Zindler and Hart, 1986). Some attention has also been focused on isotopic heterogeneity observed in certain short-lived radiogenic isotope systems (^{182}Hf-^{182}W, ^{146}Sm-^{142}Nd, ^{129}I-^{129}Xe) which indicate that some OIB have incorporated materials that formed during the first ~0.5 Ga of Earth history, and that these materials were preserved to the present (e.g., Mukhopadhyay, 2012; Mundl et al., 2017; Peters et al., 2018). These signatures provide important insights into major early Earth processes including core formation, planetary outgassing, and atmospheric loss, as well as possible magma ocean differentiation and crust-forming processes. In particular, the discovery of ^{182}W anomalies in some young, plume-derived rocks has strengthened earlier arguments for the preservation of primordial mantle reservoirs to the present that are based on, e.g., noble gas isotopic characteristics (Mukhopadhyay, 2012; Rizo et al., 2016a; Mundl et al., 2017; Mundl-Petermeier et al., 2019). Variable, negative correlations between $^{3}He/^{4}He$ and $^{182}W/^{184}W$ observed in Hawaiian, Samoan, and Icelandic lavas, further support the contention that at least these three OIB systems sample one or more primordial mantle reservoirs (Mundl et al., 2017; Mundl-Petermeier et al., 2019).

To further investigate the nature and origin of the putative primordial mantle reservoirs sampled by OIB, we report ^{182}W data for the Hf-W system (where $^{182}Hf \rightarrow {}^{182}W + 2\beta^{-}$; $t^{1/2} = 8.9$ Ma; Vockenhuber et al., 2004), in combination with previously published $^{3}He/^{4}He$ ratios on OIB from 15 different OIB and seamount systems. In order to account for one inferred mantle source reservoir composition, we assess the possibility of core-mantle equilibration processes using metal-silicate partitioning calculations, based on experimental data. We also combine the geochemical data with lower mantle seismic observations that may provide geophysical constraints on the locations of the inferred mantle source reservoirs.

2. SAMPLES

Prior studies of OIB have reported ^{182}W isotopic data from Hawaii, Samoa, Iceland, Pitcairn, Canary Islands, Mangaia, Azores, Cape Verde, Tristan da Cunha, Kerguelen and Reunion (Willbold et al., 2011; Liu et al., 2016a; Mundl et al., 2017; Mei et al., 2018; Mundl-Petermeier et al., 2019; Rizo et al., 2019). In order to expand the database for OIB and related rocks, we report new data for 35 additional samples, including ocean island basalts from Moorea (Societies), Azores, Caroline islands, Juan Fernandez, Heard, Galapagos, and Tristan da Cunha, as well as from the MacDonald seamount and the Discovery ridge anomaly, a topographic anomaly at the southern Mid-Atlantic Ridge (Sarda et al., 2000). We also report new data for additional samples from Hawaii, Samoa, and Pitcairn. By combining the data from prior studies with the new dataset, we assemble a global set of ^{182}W data for lavas comprising 70 samples from 15 hotspots (Fig. 1).

Samples range from basalts to picrites, all of which erupted between ~ 15 Ma ago and the present. Most of the samples studied for W isotopes have previously been well characterized with respect to major and trace element compositions, as well as long-lived radiogenic isotopic compositions (see supplementary material for data and references).

3. ANALYTICAL METHODS

3.1. Tungsten concentrations

Tungsten concentrations were determined by isotope dilution at the University of Maryland (UMd). Approximately 100 mg of sample powder was digested in 6 ml

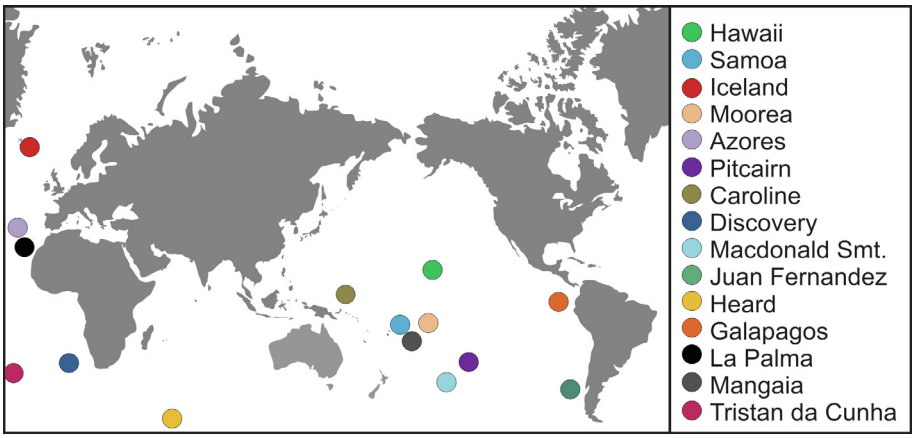

Fig. 1. World map showing all 15 studied hotspot locations.

concentrated HF:HNO_3 5:1 for 3–5 days at ~150 °C, with appropriate amounts of a ^{182}W spike. After complete dissolution was achieved, the samples were dried down and treated with a few drops of concentrated HNO_3 and 30% H_2O_2. Following another dry down, the samples were converted to chloride form by addition of 1–2 ml of 8 M HCl. After evaporation to dryness, residues were re-dissolved in 0.5 M HCl-0.5 M HF and W was separated using an anion-exchange column chemistry similar to that discussed in Kleine et al. (2004). Concentrations were measured using the *Element 2* single-collector ICP-MS at the UMd. Typical concentration uncertainties were ≤5%.

3.2. Tungsten isotopic composition

To aim for ~1 μg W load per analysis, between 0.7 and 15 grams of sample powder were digested in 30–100 ml of a 5:1 mixture of concentrated HF and HNO_3 for approximately 5 days at ~150 °C. Samples were evaporated to dryness and treated with 1–5 ml of concentrated HNO_3 and 30% H_2O_2. Following a drydown, the samples were converted to chloride form by adding 1–10 ml of 8 M HCl. After evaporation to dryness, the samples were dissolved in 10–150 ml 1 M HCl-0.1 M HF and centrifuged to avoid loading potentially-formed fluorides. Tungsten was separated from the supernatant using a four-step ion exchange chromatography method described in Peters et al. (2019). The total W recovery was between 80 and 95% for all samples.

The isotopic compositions were measured by thermal ionization mass spectrometry in negative ionization mode (N-TIMS) using a *Thermo-Fisher Triton* at the UMd. Measurements were performed using the method presented in Archer et al. (2017). In brief, W was loaded onto a single Re filament and measured as WO_3. Five μg of La and Gd each was added as electron emitter and O_2 was bled into the source at constant pressure to enhance ionization. $^{186}W^{16}O_2{}^{18}O$ and $^{187}Re^{16}O_2{}^{18}O$ were measured with every run to perform per-integration oxide interference corrections. All W isotopic ratios were corrected for instrumental mass bias by normalizing to $^{186}W/^{183}W = 0.92767$ or $^{186}W/^{184}W = 1.98594$ (Völkening et al., 1991). All data are reported as $\mu^{182}W$ and $\mu^{183}W$, which are the deviations of $^{182}W/^{184}W$ and $^{183}W/^{184}W$, respectively, of a given sample from that of the in-house *Alfa Aesar* laboratory W standard. Uncertainties in $\mu^{182}W$, based on the long-term 2SD of our *Alfa Aesar* in laboratory standard, were ±4.5. All measured $^{183}W/^{184}W$ ratios were identical within uncertainties (±6 $\mu^{183}W$ units) to the average *Alfa Aesar* standard data (Table S1).

4. RESULTS

The new data are characterized by $\mu^{182}W$ values that range from ~0 to −23 (±4.5) (Table 1, Fig. 2) and thus, include samples with the most negative $\mu^{182}W$ signatures measured to date (Fernandina, Galapagos). No resolved *positive* $\mu^{182}W$ anomalies were measured in any of the studied samples. Further, no correlations were observed between $\mu^{182}W$ and whole rock major or trace element concentrations, (including W) (Fig. 3), or with most long-lived radiogenic isotope systems (Sr, Nd, Hf, Pb, Os; Fig. S1). The sample suite exhibits a large range in W concentrations from as low as 9 ppb to 1800 ppb (Table 1). There is also no global correlation of W concentrations with major element compositions (e.g., MgO) (Fig. S2). Though trace element data are not available for all studied samples, none of the samples show enrichment in W concentrations relative to elements with similarly incompatible behaviour during mantle melting (e.g., Th), arguing against any secondary W enrichment or contamination (Fig. S3).

With the exception of the two samples from Tristan da Cunha and one from the Azores, all OIB samples examined here for W isotopes have been previously characterized for He isotopic composition. While some OIB systems, such as the Canary Islands (~8 R/R_A; Day et al., 2011; where R/R_A is the measured $^3He/^4He$ normalized to the atmospheric ratio of 1.384×10^{-6}; Mabry et al., 2013) and Mangaia (~6 R/R_A; Hanyu and Kaneoka, 1997), are characterized by uniformly low $^3He/^4He$, other OIB systems range to higher $^3He/^4He$ than is characteristic of the upper mantle, which ranges from ~7 to ~9 R/R_A (Graham, 2002). Here, He ratios in all OIB samples range from 4.5 to 40 R/R_A (Table 1), which encompasses most of the observed range for mantle derived basalts. The data in Table 1 includes samples from all of the highest $^3He/^4He$ OIB: Hawaii, Iceland, Galapapos, Samoa.

Table 1
New and previously published $\mu^{182}W$ and W concentration data, as well as previously published $^3He/^4He$. $\mu^{182}W$ is the deviation of $^{182}W/^{184}W$ of a sample from that of the average of repeated measurements of an Alfa Aesar tungsten standard. All results are presented normalized to $^{186}W/^{183}W$. New data in bold. $\mu^{182}W$ data in italics were previously published by Mundl et al. (2017) (Samoa, Hawaii, Pitcairn, La Palma, and Mangaia) and Mundl-Petermeier et al. (2019) (Iceland). 2SE and 2SD of newly measured samples refer to 2× the standard error of individual analysis (in-run statistics) and 2× the standard deviation of multiple analyses of the same sample, respectively. n.d. – not determined; dup - duplicate analysis; s.f. - second filament load; ave - average. $^3He/^4He$ data from [a]Jackson et al. (2009), [b]Jackson et al. (2014), [c]Workman et al. (2004), [d]Jackson et al. (2007), [e]same lava flow as sample OFU-04-06 from Jackson et al. (2007), [f]Brandon et al. (1999) and references therein, [g]Kurz et al. (2004), [h]Kent et al. (1999), [i]Mundl et al. (2017), [j]Williams (2005), [k]Halldórsson et al. (2016), [l]Füri et al. (2010), [m]Mundl-Petermeier et al. (2019), [n]Hanyu and Kaneoka (1997), [o]Moreira et al. (2018), [p]Garapić et al. (2015), [q]Jackson et al. (2017a,b), [r]Sarda et al. (2000), [s]Moreira and Allègre (2004), [t]Farley et al. (1993), [u]Hilton et al. (1995), [v]Kurz et al. (2014), [w]Kurz et al. (2009), [x]Geist et al. (2005), [y]average La Palma from Day et al. (2010), [z]average Mangaia from Hanyu and Kaneoka (1997).

Hotspot	Sample	$\mu^{182}W$	2SE/2SD	W [ppb]	$^3He/^4He$ [R/R_A]	1σ
Samoa	*ALIA 115-18*	*3.0*	*4.5*	*844*	*4.5*[a]	*0.04*
	AVON3-63-2	*−4.9*	*2.1*	*306*	*10.3*[b]	*0.06*
	AVON3-70-9	*−5.8*	*5.2*	*523*	*8.1*[c]	
	AVON3-71-22	*−2.8*	*4.0*	*342*	*9.6*[c]	
	AVON3-73-1	*−7.7*	*3.8*	*693*	*8.1*[c]	
	AVON3-77-1	*−7.5*	*4.5*	*720*	*13.5*[c]	
	T33	*−4.6*	*3.5*	*304*	*16.6*[c]	
	OFU-04-14	*−17.3*	*4.5*	*213*	*25.0*[d]	*0.20*
	OFU-04-15	**−10.6**	**2.6**	n.d.	*29.6*[d]	*0.20*
	OFU-04-15 s.f.	**−16.7**	**4.1**			
	OFU-04-15 ave	**−13.7**	**4.8**			
	OFU-05-18	*−13.8*	*3.3*	*414*	*33.8*[e]	*0.20*
Hawaii	*ML 1868-9*	*−0.3*	*3.1*	*162*	*8.0*[f]	*1.50*
	SR0683-5.75	**−1.8**	**4.7**	n.d.	*10.7*[g]	*0.10*
	SR0891-15.10	*−10.0*	*3.7*	*90*	*14.0*[g]	*0.10*
	SR0750-12.45	*−11.5*	*5.2*	*114*	*23.2*[g]	*0.20*
	KIL1840-2	*−11.9*	*4.4*	*230*	*13.3*[f]	*0.50*
	LO-02-02	*−11.8*	*4.5*	*173*	*31.6*[h]	*0.80*
	J2-374-R5	*−15.2*	*4.5*	*205*	*32.2*[i]	*0.80*
	SR0762-4.6	**−8.7**	**3.5**	n.d.	*19.8*[g]	*0.10*
	KOH 1-28	**−5.3**	**3.6**	**157**	*10.5*[f]	*2.00*
	ML 2-50	**−12.3**	**4.3**	**121**	*17.6*[f]	*1.00*
	MK 1-6	**−7.8**	***6.1***	*209*	*13.4*[i]	*0.35*
	LO-02-04	**−19.0**	**5.0**	**113**	*31.6*[h]	*0.70*
	LO-02-04	**−16.1**	**1.9**			
	LO-02-04	**−25.6**	**2.9**			
	LO-02-04 ave	**−20.2**	**9.7**			
Iceland	*SNS206*	*−0.6*	*4.5*	*380*	*8.5*[j]	*0.10*
	SNS214	*−0.7*	*4.5*	*398*	*7.9*[j]	*0.20*
	STAP-1	*−3.5*	*4.5*	*285*	*14.2*[k]	*0.34*
	TRI-1	*−11.2*	*4.5*	*290*	*25.3*[k]	*0.56*
	TRI-2	*−9.5*	*4.5*	*199*	*25.7*[k]	*0.62*
	A27	*−4.8*	*4.5*	*117*	*19.7*[l]	*0.32*
	408614	*−7.1*	*4.5*	*59*	*40.2*[i]	*0.70*
	408616	*−9.3*	*4.5*	*34*	*38.7*[m]	*1.00*
	408617	*−7.2*	*4.5*	*48*	*37.6*[m]	*0.80*
	ICE-14-16	*−11.7*	*4.5*	*74*	*19.8*[m]	*0.40*
	ICE-14-18	*−4.5*	*4.5*	*62*	*26.3*[m]	*0.70*
	ICE-14-27	*−6.5*	*4.5*	*49*	*36.6*[m]	*1.00*
	ICE-14-29	*−8.7*	*4.5*	*46*	*34.2*[m]	*1.00*
	ICE-14-32A	*1.7*	*4.5*	*9*	*17.8*[i]	*0.30*
	ICE-16-03	*−7.8*	*4.5*	*33*	*36.1*[m]	*1.00*
Moorea	**MO-01-01**	**−8.2**	**3.6**	**122**	*17*[n]	*1.60*
Azores	**ACO 2000-52**	**−9.9**	**4.5**	**271**	*18.4*[o]	
	116420	**1.3**	**3.2**	**347**	*n.d.*	

(*continued on next page*)

Table 1 (*continued*)

Hotspot	Sample	$\mu^{182}W$	2SE/2SD	W [ppb]	$^3He/^4He$ [R/R_A]	1σ
Pitcairn	**PIT-16**	**−10.5**	**3.5**	n.d.	*11.8*[p]	
	PIT-16	**−5.5**	**4.0**			
	PIT-16 ave	**−8.0**	**4.5**			
	PIT-1	*−2.7*	*4.0*	*385*	*8.6*[p]	
	PIT-8	*−1.9*	*4.0*	*178*	*8.0*[p]	
Caroline	KOS-13-4	**−3.6**	**4.0**	**84**	11.5[q]	*0.18*
	PON-13-13	**−3.1**	**5.0**	**150**	7.9[q]	*0.15*
	KOS-13-19	**−4.6**	**4.0**	**91**	12.8[q]	*0.21*
Discovery	EW9309 5D 5g	**−7.9**	**3.6**	**176**	14.8[r]	
	EW9309 3D 3g	**−5.2**	**2.7**	**78**	n.d.	
	EW9309 3D 3g s.f.	**−7.1**	**3.0**			
	EW9309 3D 3g ave	**−5.2**	**2.7**			
	EW9309 4D 2g	**−5.2**	**2.8**	**138**	n.d.	
	EW9309 4D 2g s.f.	**−6.9**	**3.5**			
	EW9309 4D 2g ave	**−5.2**	**2.8**			
	EW9309 3D 1g	**−6.3**	**2.8**	**139**	15.2[r]	
	EW9309 4D 3g	**−9.0**	**2.7**	**155**	14.0[r]	
MacDonald Seamount	SO47 64DS2	**−7.3**	**3.0**	**799**	15.8[s]	*0.30*
	SO47 64DS2 s.f.	**−10.1**	**3.9**			
	SO47 64DS2 ave	**−8.7**	**4.5**			
Juan Fernandez	PIN-8	**−14.7**	**3.8**	**115**	17.2[t]	
	PIN-12	**−15.6**	**2.8**	**175**	16.6[t]	
	MF-3	**−5.9**	**3.0**	**220**	8.0[t]	
Heard	HB24 A	**−18.2**	**3.4**	**950**	18.3[u]	*0.45*
	HB24 A dup	**−16.6**	**3.4**			
	HB24 A dup s.f.	**−20.2**	**4.5**			
	HB24 A ave	**−18.3**	**3.7**			
	65054	**−12.2**	**2.9**	**1035**	17.8[u]	*0.45*
	65054 s.f.	**−16.2**	**5.0**			
	65054 ave	**−14.2**	**4.5**			
	65085	**−6.3**	**2.9**	**459**	8.0[u]	*0.20*
	65085 s.f.	**−7.4**	**3.3**			
	65085 ave	**−6.3**	**4.5**			
	HD11	**−7.1**	**3.2**	**838**	7.5[u]	*0.20*
	HD11 s.f.	**−7.0**	**4.0**			
	HD11 ave	**−7.1**	**4.5**			
Galapagos	NSK97-206	**−22.7**	**3.3**	**150**	22.7[v]	*0.20*
	NSK97-214	**−20.3**	**3.5**	**227**	29.8[v]	*0.30*
	NSK97-214 dup	**−24.7**	**3.0**			
	NSK97-214 dup s.f.	**−21.1**	**3.5**			
	NSK97-214 ave	**−22.0**	**4.7**			
	NSK97-229	**−21.1**	**3.2**	**141**	27.3[v]	*0.20*
	DRFT04-D3-A	**−5.2**	**2.7**	**98**	8.26[w]	*0.06*
	DRFT04-D4-A	**−3.7**	**2.9**	**149**	8.99[w]	*0.05*
	W95-59	**−4.2**	**3.0**	**126**	9.04[x]	*0.06*
La Palma	LP-15	**0.1**	**4.0**	**855**	7.6[y]	
Mangaia	MG 1001	**−2.8**	**5.4**	**346**	6.3[z]	
	MG 1008	**2.6**	**4.0**	**305**	6.3[z]	
Tristan da Cunha	110014	**−4.4**	**3.4**	**1811**	n.d.	
	110020	**−4.8**	**3.0**	**629**	n.d.	

5. DISCUSSION

5.1. Tungsten-helium mantle heterogeneities

Continuous melt extraction from the upper mantle and subduction of materials from oceanic and continental lithosphere throughout Earth's history has produced mantle reservoirs with distinct geochemical/isotopic signatures (e.g., White and Hofmann, 1982). Consequently, rocks derived from volcanic systems that may access such residues and recycled materials are characterized by isotopic and compositional variations that extend beyond the ranges

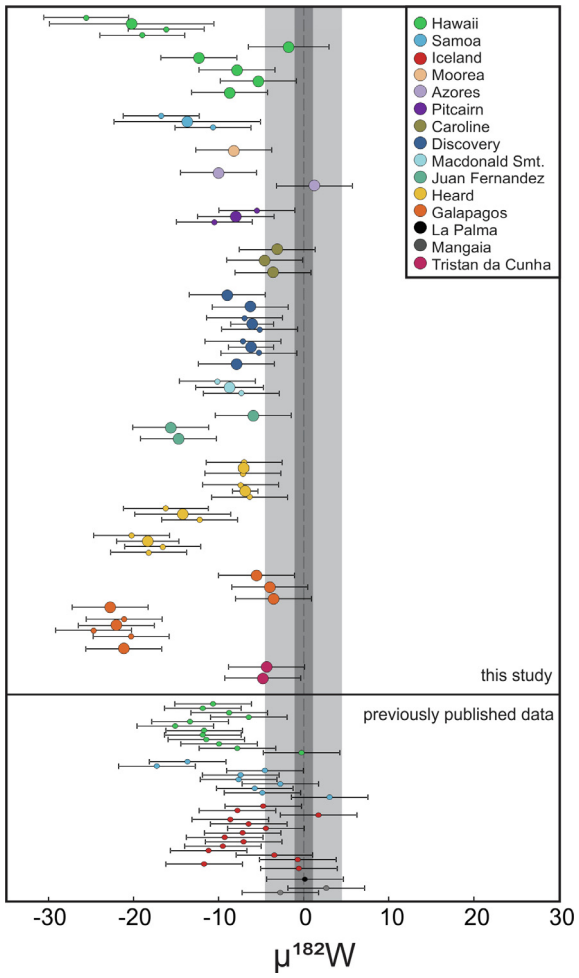

Fig. 2. $\mu^{182}W$ results of newly studied OIB samples from 15 different hotspots. Several hotspots have samples with well-resolved negative ^{182}W anomalies. Error bars of individual data represent 2SE of individual runs (Table 1) or the average 2SD of repeated analyses of *Alfa Aesar* W standard (4.5 ppm), whichever is greater. Results of samples where multiple analyses were performed are shown in smaller symbols, with their averages in larger symbols. Error bars of averages represent 2SD of multiple analyses. Dark and light grey bars are 2SE and 2SD, respectively, of repeated analyses of *Alfa Aesar* tungsten standards. Previously published data from Mundl et al. (2017) and Mundl-Petermeier et al. (2019).

observed in mid-ocean ridge basalts (MORB) (e.g., White, 2010; and references therein). Based primarily on long-lived radiogenic isotope compositions (i.e., Nd, Sr, Pb, Hf, Os), OIB sources have been interpreted to reflect contributions from at least three endmember compositional types characterized by radiogenic Pb (HIMU), or geochemically enriched Nd isotopic compositions (low $^{143}Nd/^{144}Nd$; EM1 and EM2). The geochemically depleted mantle endmember from which MORB is derived (DMM, depleted MORB mantle) serves as a fourth component (e.g., White and Hofmann, 1982; Zindler and Hart, 1986; Hart, 1988; Hofmann, 1997; Workman and Hart, 2005). In addition to long-lived radiogenic isotope compositions (Nd, Sr, Pb, Hf and Os), OIB sources differ from the DMM in having much more variable noble gas isotopic compositions. OIB (and flood basalts) are characterized by substantial variations in $^{3}He/^{4}He$ ranging from lower than MORB (<7 R/R_A) to up to 50 R/R_A, as observed in some Baffin Island and West Greenland flood basalts (e.g., Graham et al., 1998; Starkey et al., 2009). Given that ^{3}He is a primordial isotope, and ^{4}He is predominantly produced through U and Th decay, $^{3}He/^{4}He$ ratios greater than what is observed along spreading ridges are commonly interpreted to indicate contributions of He from mantle reservoirs that have undergone little or no degassing (e.g., Kurz et al., 1982; Graham, 2002). A source reservoir that has experienced little or no degassing and thus, retained most of its initial ^{3}He budget would, compared to partially degassed reservoirs, retain high $^{3}He/^{4}He$ throughout Earth's history, despite the continuous radiogenic production of ^{4}He. Supporting evidence for the existence of early-formed, little or un-degassed mantle reservoirs comes from other noble gas systems, such as Ne and Xe (e.g., Moreira, 2013; Mukhopadhyay and Parai, 2019).

The recent discovery of negative ^{182}W anomalies in modern OIB has raised new questions regarding the origin and characteristics of mantle reservoirs, as well as plume dynamics (Mundl et al., 2017; Mundl-Petermeier et al., 2019; Rizo et al., 2019). For OIB systems where sufficient He-W data are available (≥3 samples), and where He is characterized by a significant range in $^{3}He/^{4}He$, such as Hawaii, Samoa, Iceland, Pitcairn, Caroline, Juan Fernandez, Heard, and Galapagos, negative correlations between $^{3}He/^{4}He$ and $\mu^{182}W$ are observed (Fig. 4; Fig. S4). As noted by Mundl-Petermeier et al. (2019), He-W trends for Samoa, Hawaii, and *"high-Pb64"* samples from Iceland (characterized by a subset of lavas with comparatively high $^{206}Pb/^{204}Pb$) are similar, possibly suggesting the participation of components with similar $^{3}He/^{4}He$ and $\mu^{182}W$, as well as similar He and W concentrations, in the sources of the basalts. Samples from Juan Fernandez and Heard, together with samples from the Galapagos archipelago, delineate a somewhat steeper $^{3}He/^{4}He$-$\mu^{182}W$ trend. Conversely, "*low-Pb64*" basalts from Iceland (characterized by lavas with comparatively low $^{206}Pb/^{204}Pb$) define a shallower $^{3}He/^{4}He$-$\mu^{182}W$ trend. These trends with different slopes may indicate either the sampling of different endmember compositions, or different mixing proportions (Mundl-Petermeier et al., 2019).

Even though linear He-W correlations within individual OIB systems are apparent, perhaps of greater importance is the observation that the global OIB dataset lies within a triangular field when plotting $^{3}He/^{4}He$ vs. $\mu^{182}W$ (Fig. 4). To explain the He and W isotopic compositions and correlations observed for Icelandic (and also Hawaiian and Samoan) OIB, Mundl-Petermeier et al. (2019) invoked a minimum of three different mantle source components, two of which are primordial and the third similar to the DMM, at least with respect to W and He (Table 2). These components remain valid for the larger dataset reported here, and are discussed in the following sections.

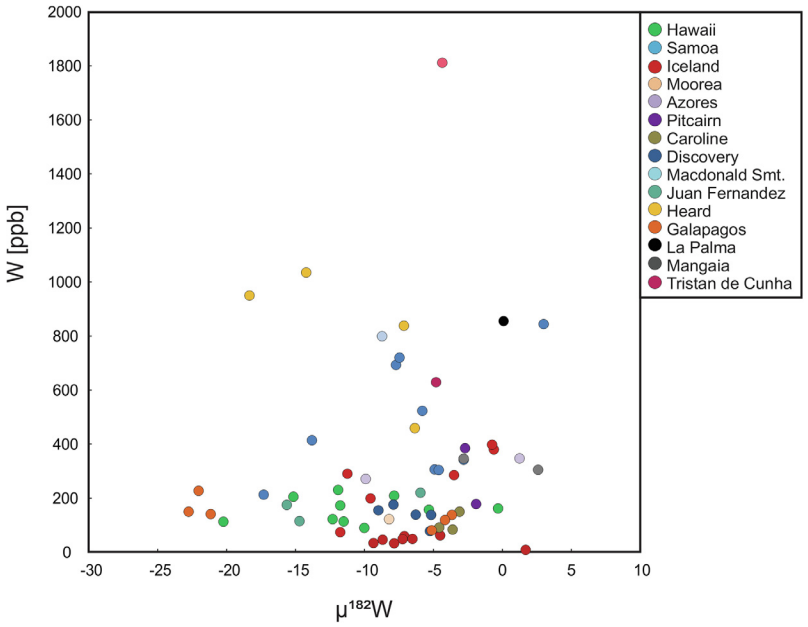

Fig. 3. $\mu^{182}W$ versus W concentrations in ppb of all samples discussed in this study. No correlation is observed in the bulk sample suite, or in samples from individual hotspots.

5.2. Characteristics and potential formation mechanisms of plume components

5.2.1. *Component 1 – Ambient Mantle (AM)*

The "ambient mantle" (*AM*) component represents major portions of Earth's mantle, including the DMM, as well as similarly degassed mid and lower mantle materials (Arevalo et al., 2013). This reservoir may have been largely homogenized with respect to W and He isotopes by convective mixing throughout Earth's 4.5 Ga history. With respect to He and W, this component is indistinguishable from the DMM, so the $\mu^{182}W$ of this component is presumed to reflect the modern upper mantle value of ~0, and have $^3He/^4He$ of 8 R/R_A, within the narrow range defined by MORB of 7 to 9 R/R_A (Graham, 2002). As W is an incompatible element that has been preferentially removed from the mantle by crust-forming processes, it is expected that W concentrations in this reservoir would be lower than the 13 ppb estimated for the bulk silicate Earth (BSE; Arevalo and McDonough, 2008). Accordingly, we assign a W concentration of 8 ppb to this mantle component. Helium concentrations in the upper mantle can be determined by estimating flux rates from the mantle to the atmosphere, and combining this with mantle melting predictions, with large uncertainties. Estimates for MORB source mantle range from 4.4×10^{-11} to 1.7×10^{-10} cc ^{3}He (STP)/g (Porcelli and Ballentine, 2002). For the mixing model we assign an intermediate ^{3}He concentration of 5.0×10^{-11} cc ^{3}He (STP)/g as an approximation. As this component may be a mixture of depleted and recycled material, major and trace element concentrations, and long-lived radiogenic isotope compositions may vary depending on the location of each OIB system.

5.2.2. *Component 2 – Early Formed Mantle Reservoir (EFMR)*

Defining the endmember compositions of W-He in the two remaining source components sampled by OIB is challenging. These compositions must be constrained using the limits placed by available data for the plume-derived samples. The highest measured $^3He/^4He$ of up to 50 R/R_A in continental flood basalts (Graham et al., 1998; Stuart et al., 2003; Starkey et al., 2009), in combination with $\mu^{182}W$ values ≈ 0 (Mundl-Petermeier et al., 2019), on the one hand, and elevated $^3He/^4He$ of up to 34 R/R_A coupled with $\mu^{182}W$ values down to -23 ± 4.5, on the other hand, require at least two distinct, little or un-degassed endmember source components. The endmember component characterized by having similar or higher $^3He/^4He$ than 50 R/R_A, and $\mu^{182}W$ value of 0 or higher will be referred to as the *Early Formed Mantle Reservoir* (*EFMR*).

The ~60 Ma flood basalts from West Greenland are characterized by $^3He/^4He$ ratios as high as 50 R/R_A and are accompanied by $\mu^{182}W$ values of ~0 in (Graham et al., 1998; Starkey et al., 2009; Mundl-Petermeier et al., 2019). Based on Pb isotopic data, Jackson et al. (2010) concluded that West Greenland rocks, as well as stratigraphically equivalent high $^3He/^4He$ Baffin Island basalts (e.g., Starkey et al., 2009), were derived from a little degassed mantle source reservoir that formed between 4.55 and 4.45 Ga. Based primarily on ^{143}Nd isotopic compositions, they concluded that this reservoir was depleted in incompatible trace elements, raising the Sm/Nd ratio. Such a reservoir could represent early crystallization products of a basal magma ocean (Labrosse et al., 2007; Coltice et al., 2011; Herzberg et al., 2013). If the isolated reservoir formed subsequent to ^{182}Hf extinction, more than ~60 Myr after

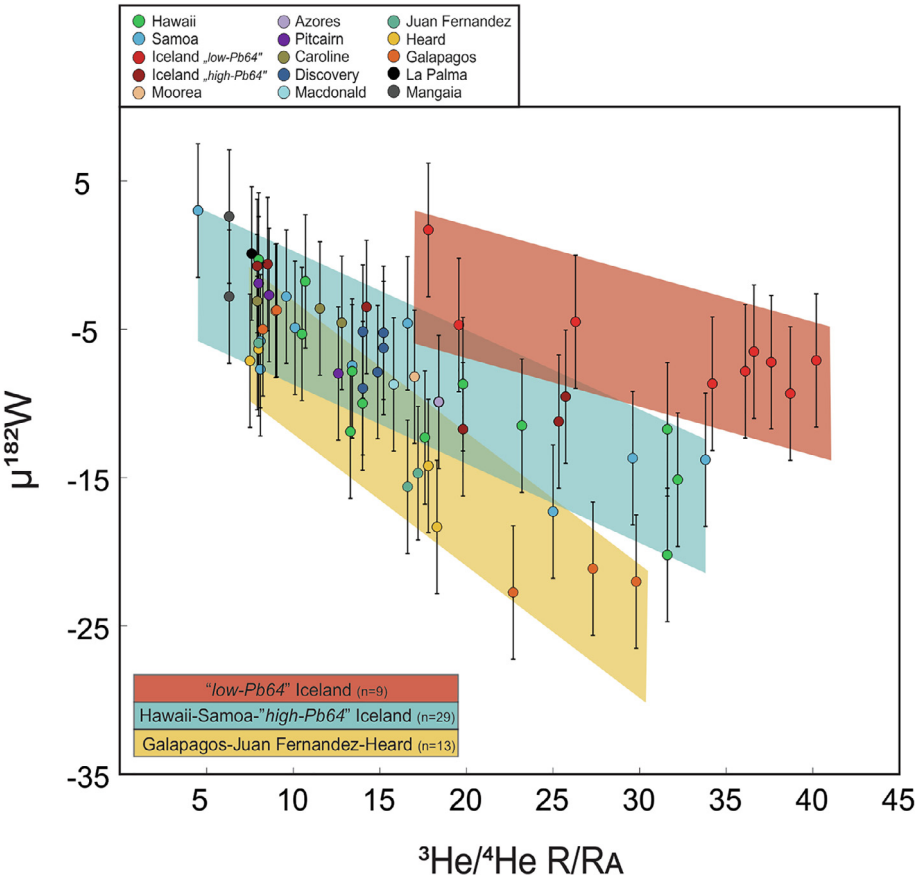

Fig. 4. Plot of $^{3}He/^{4}He$ versus $\mu^{182}W$ showing three separate He-W trends. The red trend represents the *"low-Pb64"* samples from Mundl-Petermeier et al. (2019). The light blue trend is defined by samples from Hawaii, Samoa, and the *"high-Pb64"* samples from Iceland (Mundl et al. 2017; Mundl-Petermeier et al. 2019, this study). Samples from Juan Fernandez, Heard and Galapagos make up the yellow trend (this study). Most of the OIB systems, including samples from Moorea, Azores, Pitcairn, Caroline, Discovery, Mangaia, La Palma, and Macdonald, fit the Hawaii-Samoa-*"high-Pb64"*-Iceland trend. (For interpretation of the references to colour in this figure legend, the reader is referred to the web version of this article.)

Table 2
$^{3}He/^{4}He$, He concentrations, $\mu^{182}W$, and W concentrations of individual components used in the mixing model shown in Fig. 5.

Component	Ambient mantle	Primitive reservoir	Core-mantle equilibrated IW-1.1	Core-mantle equilibrated IW-2.2	Modern SLAB	Ancient SLAB 1	Ancient SLAB 2
Abbreviation	*AM*	*EFMR*	*CMER*	*CMER*	*MRS*	*ARC+*	*ARC-*
^{4}He [cm^3 STP/g]	4.5E−06	1.2E−06	9.0E−06	9.0E−06	1.5E−05	3.0E−05	3.0E−05
^{3}He [cm^3 STP/g]	5.0E−11	1.0E−10	1.0E−09	1.0E−09	1.0E−12	1.0E−12	1.0E−12
$^{3}He/^{4}He$ [R/R_A]	8	60	80	80	0.05	0.02	0.02
$\mu^{182}W$	0	0	−220	−220	0	20	−14
W [ppb]	8	5	4500	310	10	10	10

solar system formation, it would be characterized by a $\mu^{182}W$ of 0. Silicate crystal-liquid fractionation, however, is potentially problematic in that the Baffin Island basalts are characterized by normal ^{142}Nd (de Leeuw et al., 2017). Yet, a positive ^{142}Nd signature of the source reservoir would be expected in the event of early magma ocean crystallization. Nevertheless, the proposed depleted nature and the resulting low Nd concentration of this reservoir means that any enrichment in ^{142}Nd would likely be attenuated by mixing with normal Nd in the *AM* component. Therefore, an early crystallization product remains a possible explanation. Since both the *AM* and *EFMR* endmember components have normal ^{182}W, mixing between these two endmembers will not affect the W isotopic composition.

Given these limited constraints, we assign a $^{3}He/^{4}He$ of 60 R/R_A and ^{3}He concentration of 1.0×10^{-10} cc ^{3}He (STP)/g to the *EFMR*, reflecting the incompatible element depleted and little degassed nature of the reservoir (Table 2). Further, analogous to one of the primordial source reservoirs proposed by Mundl-Petermeier et al. (2019) for the Iceland mantle plume and in accordance with results from West Greenland samples, we assume a $\mu^{182}W$ value of ~0 for this reservoir. MgSiO3 perovskite-melt distribution coefficients for W have not yet been determined. However, assuming a partitioning behavior for W similar to that of Th (MgPv/liq > 0.01) and U (MgPv/liq < 0.03; Corgne et al., 2005) in a magma ocean crystallization scenario, it is expected that an early precipitate would likely be strongly depleted in W. Thus, in our model we assign this reservoir a concentration of 5 ppb, distinctly lower than estimates for the BSE (13 ppb, Arevalo and McDonough, 2008).

5.2.3. Component 3 – Core-Mantle Equilibrated Reservoir (CMER)

The W isotopic characteristics of this endmember component, here referred to as *Core-Mantle Equilibrated Reservoir* (*CMER*), must extend below the most negative $\mu^{182}W$ value yet measured of -23 ± 4.5 (Galapagos). Thus, a mantle plume source that reflects the characteristics of the proposed third mantle reservoir must have a strongly negative $\mu^{182}W$, most likely in combination with elevated W concentration.

Some seismically identified areas at the CMB have been interpreted to be subducted crust (e.g., Tackley, 2011; Andrault et al., 2014). Associated with this, several studies have shown that Archean crust was characterized by $\mu^{182}W$ values as high as + 20 (e.g., Willbold et al., 2011; Touboul et al., 2012; Touboul et al., 2014; Willbold et al., 2015; Rizo et al., 2016b; Dale et al. 2017; Reimink et al. 2018; Tusch et al., 2019), and at least as low as −14 (Puchtel et al., 2016; Mundl et al., 2018). Consequently, one possible source of material with negative (or positive) $\mu^{182}W$ is subducted, early-formed crust. Although early subducted crust cannot be completely ruled out as the source of negative $\mu^{182}W$ in OIB, $\mu^{182}W$ signatures as low as -23 ± 4.5 in the Fernandina (Galapagos) samples require a source reservoir with a more negative W signature. Additionally, tungsten concentrations of subducted crust may also be low as a consequence of W loss by subduction fluids in the upper mantle (König et al., 2011). Thus, contributions from ancient subducted crust with negative (or positive) $\mu^{182}W$ would not significantly impact the isotopic composition of plume-derived rocks.

Another potential reservoir with an appropriate ^{182}W composition is the Earth's core. Assuming the silicate Earth has an average $\mu^{182}W = 0$, and the bulk Earth has a chondritic $\mu^{182}W$ of ~−190, mass balance requires the core to have a $\mu^{182}W = -220$ (Touboul et al., 2012). Thus, given the early formation of the core and the short lifetime of ^{182}Hf, the core is a potential source of strongly negative $\mu^{182}W$. Because some mantle plumes may originate from at or close to the CMB, the core is a strong candidate for the source of the W with negative $\mu^{182}W$. Whether a mantle plume can entrain core metal is debated (e.g., Brandon and Walker, 2005). Physical incorporation of outer core metal in a plume rising from the CMB would result in some observable geochemical effects in OIB derived from metal enriched mantle. Perhaps the most important collateral effect expected if core material becomes entrained in a mantle plume is strong enrichment of HSE (e.g., Scherstén et al., 2004; Brandon et al., 1999; Brandon and Walker, 2005). However, no obvious HSE enrichments have been detected in any OIB, including some characterized by negative $\mu^{182}W$, so direct core input into plumes seems an unlikely explanation for the negative $\mu^{182}W$ values in OIB (Ireland et al., 2009; Garapić et al., 2015; Mundl et al., 2017; Mundl-Petermeier et al., 2019; Fig. S5).

A more viable concept to explain the presence of a core isotopic signature in a mantle plume is to tap a mantle reservoir that has chemically/isotopically equilibrated with the core, and thus, may record some core-like characteristics with respect to siderophile elements, especially W isotopic composition. Isotopic equilibration between lower mantle materials and the core could take place at any time after the cessation of core formation. The resulting W concentrations and isotopic compositions strongly depend on the conditions and composition of the reservoir that equilibrates with the core. Even though recently, Yoshino et al. (in press) proposed relatively fast solid-state diffusion rates for W in the presence of highly oxidized material at the CMB, slow high-pressure diffusion rates at average modern mantle fO_2 in lower mantle phases (e.g. Holzapfel et al., 2005) argue against significant core equilibration with a solid lower mantle. Thus, a more likely scenario would be equilibration of a (partially) molten lower mantle layer with the core. This silicate layer at the CMB could potentially represent subducted oceanic crust or a remnant from an early magma ocean, complementary to early crystallites proposed to represent the *EFMR*.

To consider the effects of liquid metal – liquid silicate equilibration at the CMB we calculate the $\mu^{182}W$ value, as well as HSE, Ni, and W concentrations in the resulting silicate reservoir. For this model, we assume a silicate mass of 0.1% of the mantle, representing a thin (~5 km) layer at the CMB that equilibrates with the core (Table 3). The oxygen fugacity (fO_2) of the proposed (partially) molten silicate layer strongly affects the metal-silicate partition coefficients of the elements of interest, particularly W. Thus, we calculate W and HSE source concentrations using two different fO_2: IW-1.1 (1.1 log units below the iron-wüstite buffer) and IW-2.2 (Table 3). Approximating oxygen fugacity as $\Delta IW \approx 2 * \log_{10}\left(\frac{X_{FeO}^{silicate}}{X_{Fe}^{metal}}\right)$, where $X_{FeO}^{silicate}$ is the mole fraction of FeO in the silicate melt and X_{Fe}^{metal} is the mole fraction of Fe in the core (~0.75), the oxygen fugacities we used in our calculations roughly correspond to an iron-enriched partial melt layer with $X_{FeO}^{silicate}$ ~0.20 (IW-1.1) and a BSE composition of $X_{FeO}^{silicate}$ ~0.06 (IW-2.2) (McDonough and Sun, 1995). While a proposed fO_2 of IW-2.2 may be representative of the modern bulk mantle, a more oxidized layer at the CMB and its effects on elemental behaviour during core-mantle equilibration should also be considered. This highly oxidized layer could represent (partially) molten remnant from the crystallization of an

Table 3
Parameters used in the core-mantle equilibration calculations.

	BSE [ppm]	Core [ppm]	IW-1.1		IW-2.2	
			D (met/sil)	*CMER* [ppm]	D (met/sil)	*CMER* [ppm]
W	0.013	0.47	0.1	4.5	1.5	0.31
Pt	0.0071	5.7	20	0.28	35	0.16
Re	0.00028	0.23	500	0.00047	1700	0.00013
Ir	0.0032	2.6	1200	0.0022	4400	0.00074
Ni	1960	52,000	0.5	101,881	1.8	28,381
$\mu^{182}W$	0	−220		−220		−220

ancient basal magma ocean that resulted in significant FeO enrichment. Alternatively, it has been proposed that oxidized material, such as recycled oceanic lithosphere, may accumulate at the CMB resulting in higher fO_2 (e.g., Yoshino et al., in press).

A compositionally distinct stratified layer has been proposed to exist in the outermost outer core (e.g., Gubbins and Davies, 2013; Brodholt and Badro, 2017), but its presence and characteristics remain under debate. Therefore, we have used bulk core elemental compositions (McDonough, 2003; Table 3) to model core-mantle equilibration. For simplicity, we assume elemental concentrations of the (partially) molten silicate layer to initially reflect that of the BSE for W (13 ppb, Arevalo and McDonough, 2008) and other elements (McDonough and Sun, 1995) (Table 3). The metal-silicate partitioning of W, Pt, Re, Ir, and Ni were considered. The partition coefficient D for an element M with valence n is defined as: $D = \frac{X_M^{metal}}{X_{MO_{n/2}}^{silicate}}$. Partition coefficients were estimated at CMB conditions of 135.8 GPa and 4250 K (~100 K above the peridotite solidus, e.g., Fiquet et al., 2010) using the experimentally-derived parameterizations of Mann et al. (2012) for Pt, Re, and Ir; Fischer et al. (2015) for Ni; and Shofner et al. (2014) for W. Note that all of these parameterizations require significant extrapolations in pressure and temperature to apply at CMB conditions, especially for the HSE. Table 3 shows the estimated partition coefficients and resulting concentrations of elements in the silicate melt. Depending on fO_2, resulting W concentrations of the *CMER* can be as low as 310 ppb (IW-2.2), to as high as 4500 ppb (IW-1.1) (Table 2) and hence, are significantly enriched compared to the bulk mantle. In the equilibrated reservoir, modeled estimates of $\mu^{182}W$ for both IW-1.1 and IW-2.2 result in core-like isotopic signatures of −220. Potential collateral effects of core-mantle equilibration on other elements and resulting impact on the composition of OIB are discussed in Section 5.4.

In contrast to the molten layer representing subducted crust, a partially crystallized remnant from a magma ocean could be substantially less degassed than the convecting mantle, and thus retain high relative ^{3}He concentrations. At the same time it may also be enriched in incompatible elements, potentially resulting in high or moderate (Th + U)/He. In that case, radiogenic production of ^{4}He over 4.5 Ga would significantly lower the ^{3}He/^{4}He; however, the reservoir would still retain a higher ^{3}He/^{4}He than the convecting ambient mantle (*AM*) if the former had lower time-integrated (Th + U)/He than the latter. If core-mantle equilibration were also to significantly impact the ^{3}He abundance in *CMER*, this would likely result in distinctly higher ^{3}He/^{4}He for *CMER* compared to *AM*. Despite the ongoing debate over whether the Earth's core can be considered a potential source for noble gases, some studies have noted that the metallic reservoir may host significant amounts of He (e.g., Porcelli and Halliday. 2001; Bouhifd et al., 2013; Herzberg et al., 2013; Roth et al., 2019). The behavior of He at CMB conditions is not well constrained, and thus, it is difficult to predict the effects of core-mantle equilibration and partitioning on the ^{3}He/^{4}He of the source reservoir. Based on the composition of Jupiter's atmosphere, the core is interpreted to have an initial primordial ^{3}He/^{4}He of ~120 R/R_A (Mahaffy et al., 1998). Because no significant amounts of Th or U are expected to reside in the core, this He ratio should not have changed with time. Thus, if significant amounts of core He were transferred to the lower mantle by core-mantle equilibration, the ^{3}He/^{4}He of the CMB layer could be considerably elevated. Yet, even in this scenario, the 4.5 Ga of radiogenic ^{4}He ingrowth in a potentially (partially) molten reservoir would result in a ^{3}He/^{4}He of the CMB layer lower than that of the core: how much lower depends on the unknown time-integrated (Th + U)/He of the CMB layer. Thus, on the assumption that the *CMER* did receive significant amounts of He from the core, we assign a ^{3}He/^{4}He of 80 R/R_A and He concentrations of 1.0×10^{-09} cc ^{3}He (STP)/g to the *CMER*, which represents a mixture of He from the core and the equilibrating silicate reservoir. Further, the proposed *CMER* is characterized by a $\mu^{182}W$ of −220 and, depending on the presumed *fO2*, a W concentration of 310 ppb (Fig. 5A) or 4500 ppb (Fig. 5B). The $\mu^{182}W$ signature of the Earth's core is dependent on mass balance constraints. While Touboul et al. (2012) propose a 220 ppm deficit relative to BSE, other studies suggest a $\mu^{182}W$ of −200 for Earth's core (e.g., Kleine et al., 2009). It is important to note, that this 20 ppm uncertainty in the proposed $\mu^{182}W$ of the core has no significant effects on the proportion of the *CMER* required to explain the most negative OIB sample (Fig. S6A).

The lack of Nd in Earth's core (assuming the core is not S rich; Wohlers and Wood, 2015) means ^{142}Nd and Nd concentrations would not be affected by core-mantle equilibration. Thus, unlike W concentrations, which exhibit a ~25 to 350-fold increase during core-mantle equilibration, Nd concentrations remain constant in the *CMER*. Hence, a correlation between ^{182}W and ^{142}Nd is not expected for this

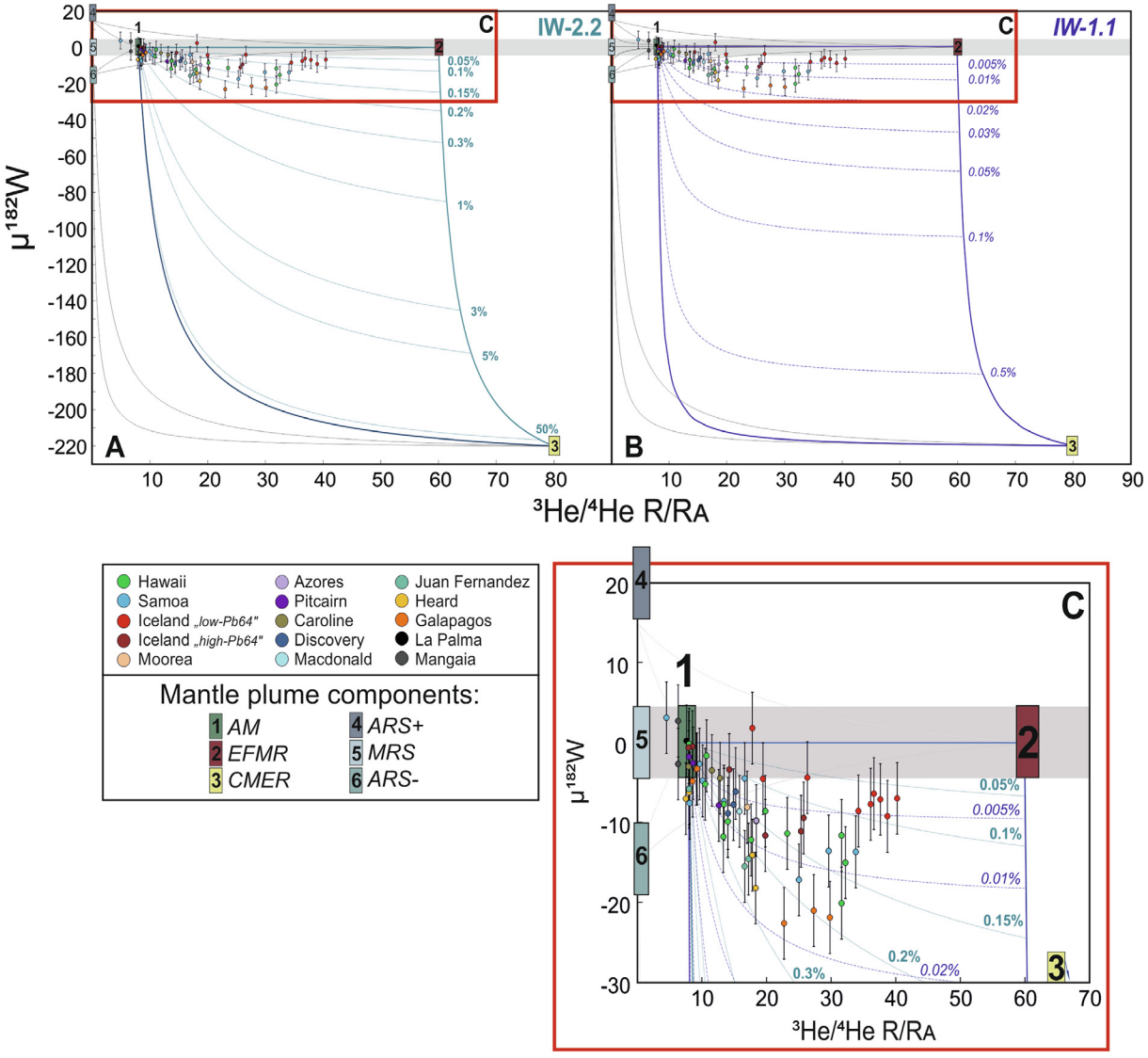

Fig. 5. Mixing model showing $^{3}He/^{4}He$ versus $\mu^{182}W$. Parameters used for mixing calculations are listed in Table 2. Numbers represent different *Components* discussed in the main text. Percentages given are the proportion of EF*MR* mixed with *CMER*. (A) *CMER* W concentrations determined by core-mantle equilibration using metal-silicate partition coefficients at IW-2.2 (B) *CMER* W concentrations determined by core-mantle equilibration using metal-silicate partition coefficients at IW-1.1. (C) Zoomed-in display of the area where samples plot. Green lines are mixing lines shown in A, blue lines represent mixing lines shown in B. Less than 0.25 % of *CMER* is necessary to explain the composition of the samples, regardless of whether the fO_2 is IW-1.1 or IW-2.2. Different proportions of *EFMR* and *CMER* are mixed with an ambient mantle (*AM*) to explain the He-W trends. *Components ARS+*, *ARS-*, and *MRS* represent ancient or modern subducted slabs with a $\mu^{182}W$ of +20, −14, and 0, respectively, that do not significantly impact the He and W isotope composition of the samples, but may explain the low $^{3}He/^{4}He$ of one sample from Samoa and two from Mangaia. Different colored symbols for Iceland represent the two sample groups classified based on Pb isotope compositions discussed in Mundl-Petermeier et al. (2019). (For interpretation of the references to colour in this figure legend, the reader is referred to the web version of this article.)

reservoir, consistent with the still-limited observations for OIB (Horan et al., 2018).

5.3. $\mu^{182}W$ vs. $^{3}He/^{4}He$ R/R_A mixing model

Generally, the $\mu^{182}W$ versus $^{3}He/^{4}He$ mixing model presented here (Fig. 5, Table 2) suggests that the main mantle plume component controlling W and He in OIB is the *EFMR*. Depending on which fO_2 is used in the core-mantle equilibration model, variable proportions of *CMER* are required to explain the negative $\mu^{182}W$ anomalies observed in some OIB. A component with a distinctly different $\mu^{182}W$ composition and considerably higher W concentrations would likely dominate the W composition of a plume-derived rock. This is shown in our mixing model, where only minor amounts of *CMER* are sufficient to explain the observed negative $\mu^{182}W$ of the most negative value of −23 from the Galapagos (Fig. 5). Even at lower

fO_2 conditions, resulting in source W concentration of only 310 ppb (IW-1.1; Table 3), less than 0.3% of *CMER* is needed to produce the most negative $\mu^{182}W$ values in samples from Galapagos. Using IW-2.2 to model source compositions resulting in source W concentrations of 4500 ppb requires even lower amounts (<0.03%) of the core-mantle equilibrated component (Fig. 5). Because of the very small amounts of *CMER* contributing to the mantle plume melt, its $^3He/^4He$ composition is not crucial, as it does not significantly affect the outcome of the mixing calculations in the upper portion of the He-W model, where OIB samples plot (Fig. 5C). Hence, whether He is also derived from the core, with high $^3He/^4He$, or whether the hypothetical melt is degassed (when derived from subducted crust) and without significant He contribution from the core is unimportant for the mixing model, as long as the molten layer has a core-like W isotopic composition and significantly higher W concentrations than the other source reservoir components (*AM* and *EFMR*; Fig. S6B). Similarly, assuming the *EFMR* component is characterized by a $\mu^{182}W$ of + 20, rather than 0 (see discussion above) will change the mixing proportions of the three main plume components only minimally (Fig. S6C).

Differently sloping He-W trends for variable OIB systems (Fig. S4) may suggest that different plumes entrain variable proportions of deep mantle sources and that the relative proportions of the components entrained by a long-lived mantle plume may change with time, as recently proposed by Jones et al. (2019) and Mundl-Petermeier et al. (2019). A single trend suggests that the amount of ambient mantle material may not be time-dependent, but may vary according to specific OIB settings. Changes in component proportions may occur on relatively short timescales, as evidenced by the Hawaiian hotspot, where different eruption events of the same volcano have led to variable $^3He/^4He$ and $\mu^{182}W$ signatures. Unlike in the Iceland mantle plume, where Mundl-Petermeier et al. (2019) recognized two separate He-W trends broadly defined by age, all Hawaiian samples examined to date plot on a single trend (Fig. S4), indicating that the *EFMR* to *CMER* ratio did not change with time, but rather was driven by the amount of incorporated *AM* material. Mantle plumes originating at different locations and times in the deep mantle, not surprisingly, likely entrain different proportions of source materials. While some plumes, like the ones beneath Heard, Juan Fernandez, and Galapagos, seem to entrain more of the core-mantle equilibrated material (*CMER*) and thus exhibit a steeper He-W correlation, the proportion of *EFMR* material may be greater in other mantle plumes, such as those of Hawaii and Samoa. Further, addition of *AM* material may vary regionally and temporally. Thus, long-lived radiogenic isotope compositions of different hotspots may reflect variations in the *AM* source.

5.4. Additional possible endmember: subducted crustal components

The He-W isotopic characteristics of three samples – ALIA115-18 (which is EM2), MG1001 and MG1008 (which are HIMU) – fall outside of the range of most OIB and require special circumstances to account for their compositions. To explore possible explanations for these compositions, we consider the effects of several additional source components on He-W isotopic systematics (Fig. 5, Table 2). The three samples from Mangaia and Samoa have $^3He/^4He$ of <7 R/R_A which is lower than typical MORB. Hence, these compositions suggest the participation of a low $^3He/^4He$ component in the formation of these plume-derived melts. One potential candidate that is characterized by low $^3He/^4He$ is subducted slab material, including oceanic crust (contributing to HIMU) and material derived from continental crust (contributing to EM2). Descending oceanic plates in the mantle may experience dehydration and/or melting in the upper mantle, or in some cases slabs may be subducted to greater depth and stored in the deep mantle. The fluid mobile element W may be depleted due to a loss to fluids produced by subduction-related dehydration reactions (e.g., König et al., 2008, 2011; Bali et al., 2012) and may thus, not be concentrated in dehydrated slabs sinking further downwards into the mantle. Additionally, as He is lost by degassing during the formation of crust and even further during the subduction process, subducted slabs are expected to have very low ^3He. Time integrated (U + Th)/He ratios of a slab component will result in significant radiogenic production of ^4He, and hence, $^3He/^4He$ ratios that are lower than MORB. Thus, a subducted slab component is likely characterized by low W concentrations (~10 ppb) and, depending on the timing of formation, positive (+20; most positive $\mu^{182}W$ signature of Archean crustal rocks), "normal" (0), or negative (−14; most negative $\mu^{182}W$ signature of Archean crustal rocks) $\mu^{182}W$ and very low $^3He/^4He$ in the range of 0.02 to 0.05 R/R_A (e.g., Van Soest et al., 1998; McCrory et al., 2016). Thus, an ancient subducted slab component with positive or negative $\mu^{182}W$, and similarly a modern subducted slab component with "normal" $\mu^{182}W$, may explain some of the lower than MORB-like $^3He/^4He$ OIB samples (Samoa, Mangaia) but would not be expected to have critical impact on the $^3He/^4He$ and ^{182}W isotopic composition of most OIB (Fig. 5). A recycled component may, however, have significant effects on long-lived radiogenic isotope compositions, such as Sr, Nd and Hf, and may be the main component responsible for the composition of OIB. An incompatible element enriched, subducted crustal component may overprint the long-lived radiogenic isotope composition of an incompatible element depleted main source (*EFMR*) without significantly affecting W and He isotopic composition. This could explain the different Sr, Nd, and Hf isotope compositions of various hotspots and the lack of correlation thereof with ^{182}W and $^3He/^4He$ (Fig. S1). As with the *AM* component, the addition of a recycled slab component may vary with the location of the OIB (Fig. 6).

5.5. Consideration of collateral effects of core-mantle interaction

Equilibrating lower mantle material with the liquid outer core would likely affect W (and He) concentrations and isotopic composition in the equilibrated silicate layer. As shown by the mixing model, addition of very low

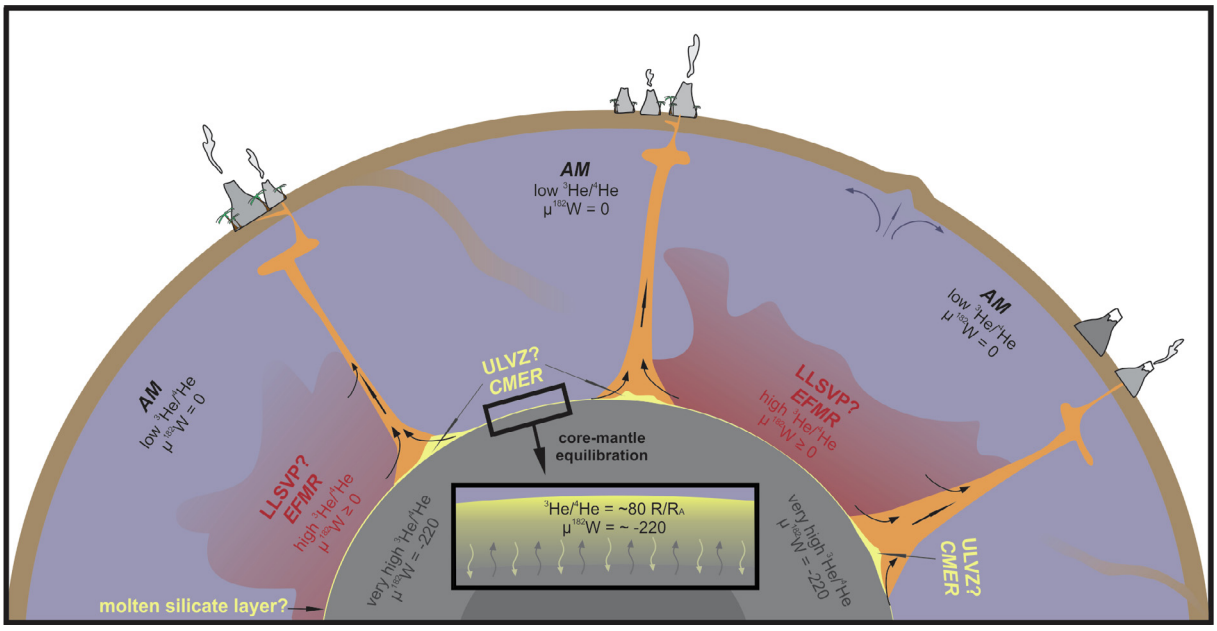

Fig. 6. Cartoon cross section through Earth's interior showing mantle plumes originating at the CMB incorporating material from different source regions in variable proportions. A thin molten layer at the CMB that may have equilibrated chemically and isotopically with the Earth's core (*CMER*) is piling up in areas where mantle plumes form, potentially representing ULVZs (after Yuan and Romanowicz, 2017). Its ^{3}He/^{4}He depends on whether the core contributed significant amounts of He during equilibration. Little or un-degassed mantle reservoirs are depicted here as LLSVPs, presumably representing our *EFMR*. The purple area represents ambient mantle material (*AM*) that has participated in mantle mixing and mantle convection processes throughout Earth's history. Displayed mantle reservoirs not to scale. *AM* – ambient mantle; *EFMR* – primordial mantle reservoir; *CMER* – core-mantle equilibrated reservoir.

amounts of a core-mantle equilibrated component strongly affects the W isotopic composition of plume derived rocks. Whether this addition of *CMER* component also has consequences for the W concentrations of OIB can be tested by looking at elements with similar incompatibilities during upper mantle melting, but that are unaffected by core-mantle equilibration (e.g., Th, U, Ta). None of the studied OIB samples that are characterized by negative μ^{182}W anomalies, indicating contribution from *CMER*, show enrichments in W over Th (Fig. S3). Despite the fact that W concentrations in *CMER* are suggested to be highly enriched (310 ppb or 4500 ppb) relative to BSE (13 ppb), the very small amounts of this plume source required to explain the W isotopic compositions of the samples with the lowest μ^{182}W signatures, have negligible effects on the W concentrations of OIB samples (Fig. S7).

In addition to W, a core-mantle equilibration may imprint other (isotopic) geochemical signatures to the plume component. For example, we estimate that core-mantle equilibration at the CMB would result in increasing Pt concentrations by a factor of ~20–40 and Ni concentrations by a factor of ~15–50 in the equilibrated silicate melt, relative to BSE, due to these elements becoming significantly less siderophile at these extreme conditions (e.g., Mann et al., 2012; Fischer et al., 2015). Concentrations of Re and Ir are not expected to change significantly, and possibly even decrease, due to their already high (presumably late-accretion-enriched) abundances in the BSE, relative to their partitioning behavior at these conditions. Unfortunately, the behavior of Os during core-mantle equilibration at CMB conditions is more difficult to constrain and would require significant extrapolation resulting in estimates with large uncertainties. Thus, effects of core-mantle equilibration on the ^{187}Re-^{187}Os or ^{190}Pt-^{186}Os system are currently impossible to assess and require additional experimental work.

While collateral effects (e.g., Pt and Ni concentrations) of a core-mantle equilibrated silicate source would be attenuated by the low proportion (<0.03 to 0.3%) necessary to explain the negative ^{182}W signatures of some OIB, addition of similarly low amounts of core metal (≤0.3%) would have significantly larger effects, especially evidenced by the HSE Ir and Pt (Fig. S7). The highly enriched concentrations in those elements in core metal compared to a core-mantle equilibrated source would lead to detectable enrichments in OIB with negative μ^{182}W signatures. For example, 0.3% addition of actual core material would result in a three-fold increase in Ir concentration. By contrast, the addition of 0.3% of *CMER* material would have insignificant impact (Fig. S7). Where data are available, none of the samples characterized with negative μ^{182}W show obvious enrichment in HSE concentrations (Fig. S5). A similar conclusion may be drawn for other elements potentially affected by core-mantle equilibration, such as other MSE besides W. If our model calculations are correct and only very small (<0.3%) amounts of core-mantle equilibrated source material are necessary to explain the observed μ^{182}W data, then trace element and other isotopic evidence of core-mantle equilibration may be limited. Because of the large concentration and isotopic differences of W between

the core and the mantle, very small amounts show resolvable core-effects, which may not be detectable in other trace element and isotopic systems.

5.6. Seismic constraints on the locations of primordial mantle reservoirs

The origin of geochemical heterogeneities can be linked to processes that should also produce seismically observable anomalies in the lower mantle. Seismic tomography and waveform modeling reveal structures with distinct elastic properties that may be candidates for hosting various geochemical reservoirs. At the largest scales, large low-shear velocity provinces (LLSVPs) dominate the structure of the lowermost mantle (e.g. Dziewonski et al., 2010; Garnero et al., 2016), accounting for 2–9% of mantle by mass (Hernlund and Houser, 2008; Cottaar and Lekic, 2016), and are spatially associated with hotspots and large igneous provinces (Thorne et al., 2004; Torsvik et al., 2006; Burke et al., 2008; Davies et al., 2015). Recently, the seismic signature of mantle plumes hosted in LLSVP regions has been interpreted to imply compositional heterogeneity (e.g., French and Romanowicz, 2015). Based on several lines of evidence, LLSVPs have been interpreted as compositionally distinct from the rest of the Earth's mantle (e.g. Garnero et al., 2016), though this interpretation has recently been questioned (Davies et al., 2015). Geodynamic models suggest that early crystallization products from a magma ocean could have led to the formation of long-lasting structures that have been preserved until today (e.g., Labrosse et al. 2007, Ballmer et al., 2016, 2017), forming dense thermochemical piles with geometry similar to those of the LLSVPs (e.g., Jellinek and Manga, 2002; McNamara and Zhong, 2005). Tackley (1998) and Tackley (2000) argued that primordial high $^{3}He/^{4}He$ may be associated with two superplumes in the deep mantle (now called LLSVPs, or thermochemical piles), and modelling efforts continue to refine this concept to include both primordial He and Ne isotopic compositions (Coltice et al., 2011). The proposed formation mechanism of the *EFMR* which results in the geochemical features required for this endmember motivates us to associate the *EFMR* component tapped by a mantle plume with LLSVPs. However, we note that this association of *EFMR* with LLSVPs would be inappropriate for alternative explanations of LLSVPs as regions of purely accumulated oceanic crust (e.g. Christensen and Hofmann, 1994) or as purely thermal in origin (e.g. Davies et al., 2015).

At much smaller scales, patch-like zones of ultra-low velocity (ULVZs) have been mapped throughout the core-mantle boundary region both in and outside of plume-forming regions (e.g., Yu and Garnero, 2018). Several disparate explanations for the geophysical properties of ULVZs have been proposed, including that they represent Fe-rich core sediments (e.g., Buffett et al., 2000), subducted banded iron formations (Dobson and Brodholt 2005), Fe-rich silicates (e.g., Wicks et al., 2010, 2017; Mao et al. 2006), molten subducted material (e.g., Andrault et al., 2014; Liu et al., 2016b), or (partially) molten residues from an ancient basal magma ocean (e.g., Rost et al. 2005; Williams and Garnero 1996). In a more recent study, Yuan and Romanowicz (2017) proposed the existence of a thin partially molten layer around the Earth's core (Fig. 6). In areas where mantle plumes form, material from this layer would pile up to be detected as ULVZs (Hernlund and Bonati, 2019), consistent with the detection of unusually large ULVZs beneath highest-flux hotspots (Hawaii: Cottaar and Romanowicz, 2012; Samoa: Thorne et al., 2013; Iceland: Yuan and Romanowicz, 2017). A potentially liquid or partially molten layer around Earth's core, and enhanced at ULVZ's, could equilibrate with the liquid outer core to result in the chemical source characteristics of our proposed *CMER*. The association of large ULVZs with OIB locations exhibiting the most negative $\mu^{182}W$ signatures motivated Mundl et al. (2017) to speculate that ULVZs could represent the mantle source with negative $\mu^{182}W$. If this hypothesis is correct, the discovery of similarly, or even more extreme negative ^{182}W anomalies at Heard, Juan Fernandez, and Galapagos may suggest the existence of ULVZs that have not yet been detected beneath these locations, further highlighting the importance of coordinated efforts between geochemistry and seismology to constrain the location of primordial reservoirs in the deep Earth.

6. CONCLUSIONS

The global ^{182}W and $^{3}He/^{4}He$ dataset collected for 70 plume-derived samples from 15 different hotspots indicates the existence of at least two primordial mantle source reservoirs preserved in the deep mantle. The triangular data distribution in a $\mu^{182}W$ vs. $^{3}He/^{4}He$ plot requires at least three different mantle sources, and suggests primordial and ambient mantle components that contribute material to rising mantle plumes in variable proportions. High $^{3}He/^{4}He$ and small negative $\mu^{182}W$ anomalies in some samples from Iceland indicate large contributions from a primordial, relatively un-degassed mantle source with "normal" $\mu^{182}W$, which we term *EFMR*. The more negative $\mu^{182}W$ values, down to -23 ± 4.5 in lavas from Fernandina volcano (Galapagos), likely result from very small (<0.3%) contributions of a source reservoir that has received its W (and potentially He) isotopic signature as a result of core-mantle equilibration. We term this reservoir *CMER*. Equilibration of a (partially) molten silicate layer with the Earth's core would result in the source characteristics required to explain the measured ^{182}W data without leading to collateral effects, such as strongly enriched HSE, which cannot be observed in any of the samples.

The geochemically heterogeneous mantle sources proposed here may be linked to mantle reservoirs with distinct seismic characteristics. If LLSVPs result from early crystallites of a large magma ocean, they could represent *EFMR* material. The smaller ULVZs detected beneath some of the studied OIB systems may represent (partially) molten material at the CMB that equilibrated with Earth's core to result in the isotopic compositions of our proposed *CMER*.

Declaration of Competing Interest

The authors declare that they have no known competing financial interests or personal relationships that could have appeared to influence the work reported in this paper.

ACKNOWLEDGEMENTS

This study was supported by NSF grant EAR-1624587 (to RJW and AMP). AMP acknowledges FWF grant V659-N29. MGJ acknowledges NSF grant EAR-1624840. MDK acknowledges NSF-OCE and EAR support for noble gas measurements. We would like to thank T. Hanyu (Moorea), M. Moreira (Azores and MacDonald), J. Barling (Heard), P. Castillo (Juan Fernandez) and D. Geist (Galapagos) for providing valuable samples. We acknowledge NSF grant OCE-1555523 (to Marine Geological Samples Laboratory) for samples from Discovery. We would like to acknowledge the Smithsonian National Museum of Natural History for providing samples 110014, 110020 and 116420. We thank C. Münker and two anonymous reviewers for their constructive reviews. A. Bouvier is thanked for the editorial handling.

APPENDIX A. SUPPLEMENTARY MATERIAL

Supplementary data to this article can be found online at https://doi.org/10.1016/j.gca.2019.12.020.

REFERENCES

Andrault D., Pesce G., Bohifd M. A., Bolfan-Casanova N., Hénot J.-M. and Mezouar M. (2014) Melting of subducted basalt at the core-mantle boundary. *Science* **344**, 892–895. https://doi.org/10.1126/science.1250466.

Archer G. J., Mundl A., Walker R. J., Worsham E. A. and Bermingham K. R. (2017) High-precision analysis of (182)W/(184)W and (183)W/(184)W by negative thermal ionization mass spectrometry: Per-integration oxide corrections using measured (18)O/(16)O. *Int. J. Mass Spectrom.* **414**, 80–86.

Arevalo R. and McDonough W. F. (2008) Tungsten geochemistry and implications for understanding the Earth's interior. *Earth Planet. Sci. Lett.* **272**(3), 656–665.

Arevalo, Jr., R., McDonough W. F., Stracke A., Willbold M., Ireland T. J. and Walker R. J. (2013) Simplified mantle architecture and distribution of radiogenic power. *Geochem. Geophys. Geosyst.* **14**, 2265–2285.

Bali E., Keppler H. and Audetat A. (2012) The mobility of W and Mo in subduction zone fluids and the Mo-W-Th-U systematics of island arc magmas. *Earth Planet. Sci. Lett.* **351–352**, 195–207.

Ballmer M. D., Schumacher L., Lekic V., Thomas C. and Ito G. (2016) Compositional layering within the large low shear-wave velocity provinces in the lower mantle. *Geochem. Geophys. Geosyst.* **17**, 5056–5077.

Ballmer M., Houser C., Hernlund J., Wentzcovitch R. M. and Hirose K. (2017) Persistence of strong silica-enriched domains in the Earth's lower mantle. *Nature Geosci* **10**, 236–240. https://doi.org/10.1038/ngeo2898.

Bouhifd M. A., Jephcoat A. P., Heber V. S. and Kelley S. P. (2013) Helium in Earth's early core. *Nat. Geosci.* **6**, 982.

Brandon A. D., Norman M. D., Walker R. J. and Morgan J. W. (1999) 186Os–187Os systematics of Hawaiian picrites. *Earth Planet. Sci. Lett.* **174**, 25–42.

Brandon A. D. and Walker R. J. (2005) The debate over core–mantle interaction. *Earth Planet. Sci. Lett.* **232**, 211–225.

Brodholt J. and Badro J. (2017) Composition of the low seismic velocity E′ layer at the top of Earth's core. *Geophys. Res. Lett.* **44**, 8303–8310.

Buffett B. A., Garnero E. J. and Jeanloz R. (2000) Sediments at the Top of Earth's Core. *Science* **290**, 1338.

Burke K., Steinberger B., Torsvik T. H. and Smethurst M. A. (2008) Plume generation zones at the margins of large low shear velocity provinces on the core–mantle boundary. *Earth Planet. Sci. Lett.* **265**, 49–60.

Christensen U. R. and Hofmann A. W. (1994) Segregation of subducted oceanic crust in the convecting mantle. *J. Geophys. Res. Solid Earth* **99**, 19867–19884.

Coltice N., Moreira M., Hernlund J. and Labrosse S. (2011) Crystallization of a basal magma ocean recorded by Helium and Neon. *Earth Planet. Sci. Lett.* **308**, 193–199.

Cottaar S. and Lekic V. (2016) Morphology of seismically slow lower-mantle structures. *Geophys. J. Int.* **207**, 1122–1136.

Cottaar S. and Romanowicz B. (2012) An unsually large ULVZ at the base of the mantle near Hawaii. *Earth Planet. Sci. Lett.* **355–356**, 213–222.

Corgne A., Liebske C., Wood B. J., Rubie D. C. and Frost D. J. (2005) Silicate perovskite-melt partitioning of trace elements and geochemical signature of a deep perovskitic reservoir. *Geochim. Cosmochim. Acta* **69**, 485–496.

Dale C. W., Kruijer T. S. and Burton K. W. (2017) Highly siderophile element and 182W evidence for a partial late veneer in the source of 3.8 Ga rocks from Isua, Greenland. *Earth Planet. Sci. Lett.* **458**, 394–404.

Davies D. R., Goes S. and Sambridge M. (2015) On the relationship between volcanic hotspot locations, the reconstructed eruption sites of large igneous provinces and deep mantle seismic structure. *Earth Planet. Sci. Lett.* **411**, 121–130.

Day J. M. D., Pearson D. G., Macpherson C. G., Lowry D. and Carracedo J. C. (2010) Evidence for distinct proportions of subducted oceanic crust and lithosphere in HIMU-type mantle beneath El Hierro and La Palma, Canary Islands. *Geochim. Cosmochim. Acta* **74**, 6565–6589.

Dobson D. P. and Brodholt J. P. (2005) Subducted banded iron formations as a source of ultralow-velocity zones at the core–mantle boundary. *Nature* **434**, 371.

Dziewonski A. M., Lekic V. and Romanowicz B. A. (2010) Mantle Anchor Structure: An argument for bottom up tectonics. *Earth Planet. Sci. Lett.* **299**, 69–79.

Farley K. A., Basu A. R. and Craig H. (1993) He, Sr and Nd isotopic variations in lavas from the juan fernandez archipelago, SE pacific. *Contrib. Miner. Petrol.* **115**, 75–87.

Farnetani C. G., Hofmann A. W. and Class C. (2012) How double volcanic chains sample geochemical anomalies from the lowermost mantle. *Earth Planet. Sci. Lett.* **359–360**, 240–247.

Fischer R. A., Nakajima Y., Campbell A. J., Frost D. J., Harries D., Langenhorst F., Miyajima N., Pollok K. and Rubie D. C. (2015) High pressure metal–silicate partitioning of Ni Co, V, Cr, Si, and O. *Geochim. Cosmochim. Acta* **167**, 177–194.

Fiquet G., Auzende A.L., Siebert J., Corgne A., Bureau H., Ozawa H. and Garbarino G. (2010). Science 17, 1516–1518. https://doi.org/10.1126/science.1192448.

French S. W. and Romanowicz B. (2015) Broad plumes rooted at the base of the Earth's mantle beneath major hotspots. *Nature* **525**, 95.

Füri E., Hilton D. R., Halldórsson S. A., Barry P. H., Hahm D., Fischer T. P. and Grönvold K. (2010) Apparent decoupling of the He and Ne isotope systematics of the Icelandic mantle: The role of He depletion, melt mixing, degassing fractionation and air interaction. *Geochim. Cosmochim. Acta* **74**, 3307–3332.

Garapić G., Jackson M. G., Hauri E. H., Hart S. R., Farley K. A., Blusztajn J. S. and Woodhead J. D. (2015) A radiogenic isotopic (He-Sr-Nd-Pb-Os) study of lavas from the Pitcairn hotspot: Implications for the origin of EM-1 (enriched mantle 1). *Lithos* **228–229**, 1–11.

Garnero E. J., McNamara A. K. and Shim S.-H. (2016) Continent-sized anomalous zones with low seismic velocity at the base of Earth's mantle. *Nat. Geosci.* **9**, 481.

Gast P. W., Tilton G. R. and Hedge C. (1964) Isotopic Composition of Lead and Strontium from Ascension and Gough Islands. *Science* **145**, 1181.

Geist D. J., Naumann T. R., Standish J. J., Kurz M. D., Harpp K. S., White W. M. and Fornari D. J. (2005) Wolf Volcano, Galápagos Archipelago: melting and magmatic evolution at the margins of a mantle plume. *J. Petrol.* **46**, 2197–2224.

Graham D. W., Larsen L. M., Hanan B. B., Storey M., Pedersen A. K. and Lupton J. E. (1998) Helium isotope composition of the early Iceland mantle plume inferred from the Tertiary picrites of West Greenland. *Earth Planet. Sci. Lett.* **160**, 241–255.

Graham D. W. (2002) Noble gas isotope geochemistry of mid-ocean ridge and ocean island basalts: characterization of mantle source reservoirs. *Rev. Mineral. Geochem.* **47**, 247–317.

Gubbins D. and Davies C. J. (2013) The stratified layer at the core–mantle boundary caused by barodiffusion of oxygen, sulphur and silicon. *Phys. Earth Planet. Inter.* **215**, 21–28.

Halldórsson S. A., Barnes J. D., Stefánsson Andr, Hilton D. R., Hauri E. H. and Marshall Edward W. (2016) Subducted lithosphere controls halogen enrichments in the Iceland mantle plume source. *Geology* **44**, 679–682.

Hanyu T. and Kaneoka I. (1997) The uniform and low 3He/4He ratios of HIMU basalts as evidence for their origin as recycled materials. *Nature* **390**, 273–276.

Hart S. R. (1988) Heterogeneous mantle domains: signatures, genesis and mixing chronologies. *Earth Planet. Sci. Lett.* **90**, 273–296.

Hauri E. H. and Hart S. R. (1993) ReOs isotope systematics of HIMU and EMII oceanic island basalts from the south Pacific Ocean. *Earth Planet. Sci. Lett.* **114**, 353–371.

Hernlund J. W. and Bonati I. (2019) Modeling ultralow velocity zones as a thin chemically distinct dense layer at the core-mantle boundary. *J. Geophys. Res. Solid Earth* **124**, 7902–7917.

Hernlund J. W. and Houser C. (2008) On the statistical distribution of seismic velocities in Earth's deep mantle. *Earth Planet. Sci. Lett.* **265**, 423–437.

Herzberg C., Asimow P. D., Ionov D. A., Vidito C., Jackson M. G. and Geist D. (2013) Nickel and helium evidence for melt above the core–mantle boundary. *Nature* **493**, 393.

Hilton D. R., Barling J. and Wheller G. E. (1995) Effect of shallow-level contamination on the helium isotope systematics of ocean-island lavas. *Nature* **373**, 330–333.

Hofmann A. W. (1997) Mantle geochemistry: the message from oceanic volcanism. *Nature* **385**, 219–229.

Hofmann A. W. and White W. M. (1982) Mantle plumes from ancient oceanic crust. *Earth Planet. Sci. Lett.* **57**, 421–436.

Holzapfel C., Rubie D. C., Frost D. J. and Langenhorst F. (2005) Fe-Mg Interdiffusion in (Mg, Fe)Si_O3 Perovskite and Lower Mantle Reequilibration. *Science* **309**, 1707.

Horan M. F., Carlson R. W., Walker R. J., Jackson M., Garçon M. and Norman M. (2018) Tracking Hadean processes in modern basalts with 142-Neodymium. *Earth Planet. Sci. Lett.* **484**, 184–191.

Ireland T. J., Walker R. J. and Garcia M. O. (2009) Highly siderophile element and 187Os isotope systematics of Hawaiian picrites: Implications for parental melt composition and source heterogeneity. *Chem. Geol.* **260**, 112–128.

Jackson M. G., Hart S. R., Koppers A. A. P., Staudigel H., Konter J., Blusztajn J., Kurz M. and Russell J. A. (2007) The return of subducted continental crust in Samoan lavas. *Nature* **448**, 684.

Jackson M. G., Kurz M. D. and Hart S. R. (2009) Helium and neon isotopes in phenocrysts from Samoan lavas: Evidence for heterogeneity in the terrestrial high 3He/4He mantle. *Earth Planet. Sci. Lett.* **287**, 519–528.

Jackson M. G., Carlson R. W., Kurz M. D., Kempton P. D., Francis D. and Blusztajn J. (2010) Evidence for the survival of the oldest terrestrial mantle reservoir. *Nature* **466**, 853.

Jackson M. G., Hart S. R., Konter J. G., Kurz M. D., Blusztajn J. and Farley K. A. (2014) Helium and lead isotopes reveal the geochemical geometry of the Samoan plume. *Nature* **514**, 355.

Jackson M. G., Konter J. G. and Becker T. W. (2017a) Primordial helium entrained by the hottest mantle plumes. *Nature* **542**, 340.

Jackson M. G., Price A. A., Blichert-Toft J., Kurz M. D. and Reinhard A. A. (2017b) Geochemistry of lavas from the Caroline hotspot, Micronesia: Evidence for primitive and recycled components in the mantle sources of lavas with moderately elevated 3He/4He. *Chem. Geol.* **455**, 385–400.

Jellinek A. M. and Manga M. (2002) The influence of a chemical boundary layer on the fixity, spacing and lifetime of mantle plumes. *Nature* **418**, 760–763.

Jones T. D., Davies D. R. and Sossi P. A. (2019) Tungsten isotopes in mantle plumes: Heads it's positive, tails it's negative. *Earth Planet. Sci. Lett.* **506**, 255–267.

Kent A. J., Clague D. A., Honda M., Stolper E. M., Hutcheon I. D. and Norman M. D. (1999) Widespread assimilation of a seawater-derived component at Loihi Seamount, Hawaii. *Geochim. Cosmochim. Acta* **63**, 2749–2761.

Kleine T., Mezger K., Münker C., Palme H. and Bischoff A. (2004) 182Hf-182W isotope systematics of chondrites, eucrites, and martian meteorites: Chronology of core formation and early mantle differentiation in Vesta and Mars. *Geochim. Cosmochim. Acta* **68**, 2935–2946.

Kleine T., Touboul M., Bourdon B., Nimmo F., Mezger K., Palme H., Jacobsen S. J., Yin Q.-Z. and Halliday A. N. (2009) Hf-W chronology of the accretion and early evolution of asteroids and terrestrial planets. *Geochim. Cosmochim. Acta* **73**, 5150–5188.

König S., Münker C., Schuth S. and Garbe-Schönberg D. (2008) Mobility of tungsten in subduction zones. *Earth Planet. Sci. Lett.* **274**, 82–92.

König S., Münker C., Hohl S., Paulick H., Barth H. R., Lagos M., Pfander J. and Bühl A. (2011) The Earth's tungsten budget during mantle melting and crust formation. *Geochim. Cosmochim. Acta* **75**, 2119–2136.

Kurz M. D., Jenkins W. J. and Hart S. R. (1982) Helium isotopic systematics of oceanic islands and mantle heterogeneity. *Nature* **297**, 43–47.

Kurz M. D., Curtice J., Fornari D., Geist D. and Moreira M. (2009) Primitive neon from the center of the Galápagos hotspot. *Earth Planet. Sci. Lett.* **286**, 23–34.

Kurz M. D., Curtice J., Lott, III, D. E. and Solow A. (2004) Rapid helium isotopic variability in Mauna Kea shield lavas from the Hawaiian Scientific Drilling Project. *Geochem. Geophys. Geosyst.* **5**.

Kurz M. D., Rowland S. K., Curtice J., Saal A. E. and Naumann T. (2014) Eruption rates for Fernandina Volcano. In *The Galápagos American Geophysical Union (AGU)*, pp. 41–54.

Labrosse S., Hernlund J. W. and Coltice N. (2007) A crystallizing dense magma ocean at the base of the Earth's mantle. *Nature* **450**, 866.

de Leeuw G. A. M., Ellam R. M., Stuart F. M. and Carlson R. W. (2017) 142Nd/144Nd inferences on the nature and origin of the

source of high 3He/4He magmas. *Earth Planet. Sci. Lett.* **472**, 62–68.

Liu Jiachao, Li J., Hrubiak R. and Smith J. S. (2016a) Origins of ultralow velocity zones through slab-derived metallic melt. *Proc. Natl. Acad. Sci. USA* **113**, 5547.

Liu Jingao, Touboul M., Ishikawa A., Walker R. J. and Graham Pearson D. (2016b) Widespread tungsten isotope anomalies and W mobility in crustal and mantle rocks of the Eoarchean Saglek Block, northern Labrador, Canada: Implications for early Earth processes and W recycling. *Earth Planet. Sci. Lett.* **448**, 13–23.

Mabry J., Lan T., Burnard P. and Marty B. (2013) High-precision helium isotope measurements in air. *J. Anal. At. Spectrom.* **28**, 1903–1910.

Mahaffy P. R., Donahue T. M., Atreya S. K., Owen T. C. and Niemann H. B. (1998) Galileo Probe Measurements of D/H and 3He/4He in Jupiter's Atmosphere. *Space Sci. Rev.* **84**, 251–263.

Mann U., Frost D. J., Rubie D. C., Becker H. and Audétat A. (2012) Partitioning of Ru, Rh, Pd, Re, Ir and Pt between liquid metal and silicate at high pressures and high temperatures - Implications for the origin of highly siderophile element concentrations in the Earth's mantle. *Geochim. Cosmochim. Acta* **84**, 593–613.

Mao W. L., Mao H., Sturhahn W., Zhao J., Prakapenka V. B., Meng Y., Shu J., Fei Y. and Hemley R. J. (2006) Iron-Rich Post-Perovskite and the Origin of Ultralow-Velocity Zones. *Science* **312**, 564.

McCrory P. A., Constantz J. E., Hunt A. G. and Blair J. L. (2016) Helium as a tracer for fluids released from Juan de Fuca lithosphere beneath the Cascadia forearc. *Geochem. Geophys. Geosyst.* **17**, 2434–2449.

McDonough W. F. and Sun S.-S. (1995) The composition of the Earth. *Chem. Geol.* **120**, 223–253.

McDonough W. F. (2003) Compositional Model for the Earth's Core. *Treat. Geochem.*, 547–568. https://doi.org/10.1016/B0-08-043751-6/02015-6.

McNamara A. K. and Zhong S. (2005) Thermochemical structures beneath Africa and the Pacific Ocean. *Nature* **437**, 1136–1139.

Mei Q.-F., Yang J.-H. and Yang Y.-H. (2018) An improved extraction chromatographic purification of tungsten from a silicate matrix for high precision isotopic measurements using MC-ICPMS. *J. Anal. At. Spectrom.* **33**, 569–577.

Montelli R., Nolet G., Dahlen F. A., Masters G., Engdahl E. R. and Hung S.-H. (2004) Finite-Frequency Tomography Reveals a Variety of Plumes in the Mantle. *Science* **303**, 338.

Moreira M. (2013) Noble Gas Constraints on the Origin and Evolution of Earth's Volatiles. *Geochem. Perspect.* **2**, 229–230.

Moreira M. A., Madureira P. and Mata J. (2018) Noble Gas Constraints on the Origin of the Azores Hotspot. In *Volcanoes of the Azores: Revealing the Geological Secrets of the Central Northern Atlantic Islands* (eds. U. Kueppers and C. Beier). Springer, Berlin, Heidelberg, pp. 281–299.

Moreira M. and Allègre C. (2004) Helium isotopes on the Macdonald seamount (Austral chain): constraints on the origin of the superswell. *C.R. Geosci.* **336**, 983–990.

Mukhopadhyay S. (2012) Early differentiation and volatile accretion recorded in deep-mantle neon and xenon. *Nature* **486**, 101.

Mukhopadhyay S. and Parai R. (2019) Noble Gases: A Record of Earth's Evolution and Mantle Dynamics. *Annu. Rev. Earth Planet. Sci.* **47**, 389–419.

Mundl A., Touboul M., Jackson M. G., Day J. M. D., Kurz M. D., Lekic V., Helz R. T. and Walker R. J. (2017) Tungsten-182 heterogeneity in modern ocean island basalts. *Science* **356**, 66.

Mundl A., Walker R. J., Reimink J. R., Rudnick R. L. and Gaschnig R. M. (2018) Tungsten-182 in the upper continental crust: Evidence from glacial diamictites. *Chem. Geol.* **494**, 144–152.

Mundl-Petermeier A., Walker R. J., Jackson M. G., Blichert-Toft J., Kurz M. D. and Halldórsson S. A. (2019) Temporal evolution of primordial tungsten-182 and 3He/4He signatures in the Iceland mantle plume. *Chem. Geol.* **525**, 245–259.

Peters B. J., Carlson R. W., Day J. M. D. and Horan M. F. (2018) Hadean silicate differentiation preserved by anomalous 142Nd/144Nd ratios in the Réunion hotspot source. *Nature* **555**, 89.

Peters B. J., Mundl-Petermeier A., Horan M. F., Carlson R. W. and Walker R. J. (2019) Chemical Separation of Tungsten and Other Trace Elements for TIMS Isotope Ratio Measurements Using Organic Acids. *Geostand. Geoanal. Res.* **43**, 245–259.

Porcelli D. and Ballentine C. J. (2002) Models for Distribution of Terrestrial Noble Gases and Evolution of the Atmosphere. *Rev. Mineral. Geochem.* **47**, 411–480.

Porcelli D. and Halliday A. (2001) The core as a possible source of mantle helium. *Earth Planet. Sci. Lett.* **192**, 45–56.

Puchtel I. S., Blichert-Toft J., Touboul M., Horan M. F. and Walker R. J. (2016) The coupled 182W–142Nd record of early terrestrial mantle differentiation. *Geochem. Geophys. Geosyst.* **17**, 2168–2193.

Reimink J. R., Chacko T., Carlson R. W., Shirey S. B., Liu J., Stern R. A., Bauer A. M., Pearson D. G. and Heaman L. M. (2018) Petrogenesis and tectonics of the Acasta Gneiss Complex derived from integrated petrology and 142Nd and 182W extinct nuclide-geochemistry. *Earth Planet. Sci. Lett.* **494**, 12–22.

Rizo H., Walker R. J., Carlson R. W., Horan M. F., Mukhopadhyay S., Manthos V., Francis D. and Jackson M. G. (2016a) Preservation of Earth-forming events in the tungsten isotopic composition of modern flood basalts. *Science* **352**, 809.

Rizo H., Walker R. J., Carlson R. W., Touboul M., Horan M. F., Puchtel I. S., Boyet M. and Rosing M. T. (2016b) Early Earth differentiation investigated through 142Nd, 182W, and highly siderophile element abundances in samples from Isua, Greenland. *Geochim. Cosmochim. Acta* **175**, 319–336.

Rizo H., Andrault D., Bennett N. R., Humayun M., Brandon A., Vlastelic I., Moine B., Poirier A., Bouhifd M. A. and Murphy D. T. (2019) 182W evidence for core-mantle interaction in the source of mantle plumes. *Geochem. Perspect. Lett.* **11**, 6–11.

Rost S., Garnero E. J., Williams Q. and Manga M. (2005) Seismological constraints on a possible plume root at the core–mantle boundary. *Nature* **435**, 666.

Roth A. S. G., Liebske C., Maden C., Burton K. W., Schönbächler M. and Busemann H. (2019) The primordial He budget of the Earth set by percolative core formation in planetesimals. *Geochem. Perspect. Lett.* **9**, 26–31.

Sarda P., Moreira M., Staudacher T., Schilling J.-G. and Allègre C. J. (2000) Rare gas systematics on the southernmost Mid-Atlantic Ridge: Constraints on the lower mantle and the Dupal source. *J. Geophys. Res. Solid Earth* **105**, 5973–5996.

Scherstén A., Elliott T., Hawkesworth C. and Norman M. (2004) Tungsten isotope evidence that mantle plumes contain no contribution from the Earth's core. *Nature* **427**, 234.

Shofner G. A., Campbell A. J., Danielson L., Rahman Z. and Righter K. (2014) Metal-Silicate Partitioning of Tungsten from 10 to 50 GPa. *Presented at the 45th Lunar and Planetary Science Conference; 17-21 Mar. 2014; The Woodlands, TX; United States*.

van Soest M. C., Hilton D. R. and Kreulen R. (1998) Tracing crustal and slab contributions to arc magmatism in the lesser antilles island arc using helium and carbon relationships in geothermal fluids. *Geochim. Cosmochim. Acta* **62**, 3323–3335.

Starkey N. A., Stuart F. M., Ellam R. M., Fitton J. G., Basu S. and Larsen L. M. (2009) Helium isotopes in early Iceland plume

picrites: Constraints on the composition of high 3He/4He mantle. *Earth Planet. Sci. Lett.* **277**, 91–100.

Stuart F., Lass-Evans S., Godfrey Fitton J. and Ellam R. B. (2003) High $^{3}He/^{4}He$ ratios in picritic basalts from Baffin Island and the role of a mixed reservoir in mantle plumes. *Nature* **424**, 57–59.

Tackley P. J. (1998) Self-consistent generation of tectonic plates in three-dimensional mantle convection. *Earth Planet. Sci. Lett.* **157**, 9–22.

Tackley P. J. (2000) Mantle convection and plate tectonics: toward an integrated physical and chemical theory. *Science* **288**, 2002.

Tackley P. J. (2011) Living dead slabs in 3-D: The dynamics of compositionally-stratified slabs entering a "slab graveyard" above the core-mantle boundary. *Phys. Earth Planet. Inter.* **188**, 150–162.

Thorne M. S., Garnero E. J. and Grand S. P. (2004) Geographic correlation between hot spots and deep mantle lateral shear-wave velocity gradients. *Phys. Earth Planet. Inter.* **146**, 47–63.

Thorne M. S., Garnero E. J., Jahnke G., Igel H. and McNamara A. K. (2013) Mega ultra low velocity zone and mantle flow. *Earth Planet. Sci. Lett.* **364**, 59–67. https://doi.org/10.1016/j.epsl.2012.12.034.

Torsvik T. H., Smethurst M. A., Burke K. and Steinberger B. (2006) Large igneous provinces generated from the margins of the large low-velocity provinces in the deep mantle. *Geophys. J. Int.* **167**, 1447–1460.

Touboul M., Liu J., O'Neil J., Puchtel I. S. and Walker R. J. (2014) New insights into the Hadean mantle revealed by 182W and highly siderophile element abundances of supracrustal rocks from the Nuvvuagittuq Greenstone Belt, Quebec, Canada. *Chem. Geol.* **383**, 63–75.

Touboul M., Puchtel I. S. and Walker R. J. (2012) ^{182}W evidence for long-term preservation of early mantle differentiation products. *Science* **335**, 1065.

Tusch J., Sprung P., van de Löcht J., Hoffmann J. E., Boyd A. J., Rosing M. T. and Münker C. (2019) Uniform 182W isotope compositions in Eoarchean rocks from the Isua region, SW Greenland: the role of early silicate differentiation and missing late veneer. *Geochim. Cosmochim. Acta* **257**, 284–310.

Vockenhuber C., Bichler M., Golser R., Kutschera W., Priller A., Steier P. and Winkler S. (2004) 182Hf, a new isotope for AMS. *Nucl. Instrum. Methods Phys. Res., Sect. B* **223–224**, 823–828.

Völkening J., Köppe M. and Heumann K. G. (1991) Tungsten isotope ratio determinations by negative thermal ionization mass spectrometry. *Int. J. Mass Spectrom. Ion Processes* **107**, 361–368.

Weis D., Garcia M. O., Rhodes J. M., Jellinek M. and Scoates J. S. (2011) Role of the deep mantle in generating the compositional asymmetry of the Hawaiian mantle plume. *Nat. Geosci.* **4**, 831.

White W. M. and Hofmann A. W. (1982) Sr and Nd isotope geochemistry of oceanic basalts and mantle evolution. *Nature* **296**, 821–825.

White W. M. (2010) Oceanic Island Basalts and Mantle Plumes: The Geochemical Perspective. *Annu. Rev. Earth Planet. Sci.* **38** (1), 133–160. https://doi.org/10.1146/annurev-earth-040809-152450.

Wicks J. K., Jackson J. M. and Sturhahn W. (2010) Very low sound velocities in iron-rich (Mg, Fe)O: Implications for the core-mantle boundary region. *Geophys. Res. Lett.* **37**.

Wicks J., Jackson J. M., Sturhahn W. and Zhang D. (2017) Sound velocity and density of magnesiowüstites: Implications for ultralow-velocity zone topography. *Geophys. Res. Lett.* **44**, 2148–2158. https://doi.org/10.1002/2016GL071225.

Willbold M., Elliott T. and Moorbath S. (2011) The tungsten isotopic composition of the Earth's mantle before the terminal bombardment. *Nature* **477**, 195.

Willbold M., Mojzsis S. J., Chen H.-W. and Elliott T. (2015) Tungsten isotope composition of the Acasta Gneiss Complex. *Earth Planet. Sci. Lett.* **419**, 168–177.

Williams A. J. (2005) The Nature of the Chemically Enriched Components of the Iceland Mantle Plume. PhD Thesis. URI http://hdl.handle.net.uaccess.univie.ac.at/1842/14667

Williams Q. and Garnero E. J. (1996) Seismic Evidence for Partial Melt at the Base of Earth's Mantle. *Science* **273**, 1528.

Wohlers A. and Wood B. J. (2015) A Mercury-like component of early Earth yields uranium in the core and high mantle 142Nd. *Nature* **520**, 337.

Workman R. K. and Hart S. R. (2005) Major and trace element composition of the depleted MORB mantle (DMM). *Earth Planet. Sci. Lett.* **231**, 53–72.

Workman R. K., Hart S. R., Jackson M., Regelous M., Farley K. A., Blusztajn J., Kurz M. and Staudigel H. (2004) Recycled metasomatized lithosphere as the origin of the Enriched Mantle II (EM2) end-member: Evidence from the Samoan Volcanic Chain. *Geochem. Geophys. Geosyst.* **5**, 1–44.

Yoshino T., Makino Y., Suzuki T. and Hirata T. (in press) Grain boundary diffusion of W in lower mantle phase with implications for isotopic heterogeneity in oceanic island basalts by core-mantle interactions. *Earth Planet. Sci. Lett.*. https://doi.org/10.1016/j.epsl.2019.115887, in press.

Yu S. and Garnero E. J. (2018) Ultralow velocity zone locations: a global assessment. *Geochem. Geophys. Geosyst.* **19**, 396–414.

Yuan K. and Romanowicz B. (2017) Seismic evidence for partial melting at the root of major hot spot plumes. *Science* **357**, 393.

Zindler A. and Hart S. (1986) Chemical geodynamics. *Annu. Rev. Earth Planet. Sci.* **14**, 493–571.

Associate editor: Audrey Bouvier